

University of Windsor

## Scholarship at UWindor

---

Electronic Theses and Dissertations

Theses, Dissertations, and Major Papers

---

2004

### Experimental measurement of active control of intake noise.

Helen J. Ule

*University of Windsor*

Follow this and additional works at: <https://scholar.uwindsor.ca/etd>

---

#### Recommended Citation

Ule, Helen J., "Experimental measurement of active control of intake noise." (2004). *Electronic Theses and Dissertations*. 2027.

<https://scholar.uwindsor.ca/etd/2027>

This online database contains the full-text of PhD dissertations and Masters' theses of University of Windsor students from 1954 forward. These documents are made available for personal study and research purposes only, in accordance with the Canadian Copyright Act and the Creative Commons license—CC BY-NC-ND (Attribution, Non-Commercial, No Derivative Works). Under this license, works must always be attributed to the copyright holder (original author), cannot be used for any commercial purposes, and may not be altered. Any other use would require the permission of the copyright holder. Students may inquire about withdrawing their dissertation and/or thesis from this database. For additional inquiries, please contact the repository administrator via email ([scholarship@uwindsor.ca](mailto:scholarship@uwindsor.ca)) or by telephone at 519-253-3000ext. 3208.

## INFORMATION TO USERS

This manuscript has been reproduced from the microfilm master. UMI films the text directly from the original or copy submitted. Thus, some thesis and dissertation copies are in typewriter face, while others may be from any type of computer printer.

**The quality of this reproduction is dependent upon the quality of the copy submitted.** Broken or indistinct print, colored or poor quality illustrations and photographs, print bleedthrough, substandard margins, and improper alignment can adversely affect reproduction.

In the unlikely event that the author did not send UMI a complete manuscript and there are missing pages, these will be noted. Also, if unauthorized copyright material had to be removed, a note will indicate the deletion.

Oversize materials (e.g., maps, drawings, charts) are reproduced by sectioning the original, beginning at the upper left-hand corner and continuing from left to right in equal sections with small overlaps.

Photographs included in the original manuscript have been reproduced xerographically in this copy. Higher quality 6" x 9" black and white photographic prints are available for any photographs or illustrations appearing in this copy for an additional charge. Contact UMI directly to order.

ProQuest Information and Learning  
300 North Zeeb Road, Ann Arbor, MI 48106-1346 USA  
800-521-0600

UMI<sup>®</sup>



**EXPERIMENTAL INVESTIGATION OF DIELECTRIC STRENGTH  
OF POLYMER FILMS**

By

Syed Zaki Jafri

A Thesis

Submitted to the Faculty of Graduate Studies and Research  
Through the Department of Electrical and Computer Engineering  
In Partial Fulfillment of the Requirements  
For the Degree of Master of Applied Science  
At the University of Windsor

Windsor, Ontario, Canada

2001



National Library  
of Canada

Acquisitions and  
Bibliographic Services

395 Wellington Street  
Ottawa ON K1A 0N4  
Canada

Bibliothèque nationale  
du Canada

Acquisitions et  
services bibliographiques

395, rue Wellington  
Ottawa ON K1A 0N4  
Canada

*Your file Votre référence*

*Our file Notre référence*

The author has granted a non-exclusive licence allowing the National Library of Canada to reproduce, loan, distribute or sell copies of this thesis in microform, paper or electronic formats.

The author retains ownership of the copyright in this thesis. Neither the thesis nor substantial extracts from it may be printed or otherwise reproduced without the author's permission.

L'auteur a accordé une licence non exclusive permettant à la Bibliothèque nationale du Canada de reproduire, prêter, distribuer ou vendre des copies de cette thèse sous la forme de microfiche/film, de reproduction sur papier ou sur format électronique.

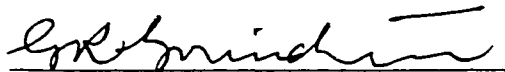
L'auteur conserve la propriété du droit d'auteur qui protège cette thèse. Ni la thèse ni des extraits substantiels de celle-ci ne doivent être imprimés ou autrement reproduits sans son autorisation.

0-612-62224-X

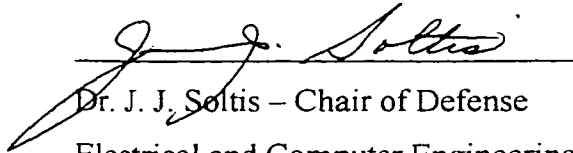
Canada

© 2001 Syed Zaki Jafri

APPROVED BY:



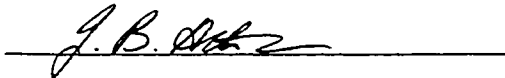
Dr. G. R. Govinda Raju – Supervisor  
Head of Electrical and Computer Engineering Dept.



Dr. J. J. Soltis – Chair of Defense  
Electrical and Computer Engineering Dept.



Prof. P. H. Alexander  
Electrical and Computer Engineering Dept.



Dr. J. B. Atkinson  
External Reader, Physics Dept.

## ABSTRACT

The dielectric strength of an insulating material does not have a fixed value but depends on several external factors which cause the strength to vary considerably depending on the system application.

This study investigates the dielectric strength of various polymers at different temperatures using an experimental setup where sufficient data is collected to merit and validate the use of statistical techniques in determining the dielectric strength. The results achieved are interpreted in terms of probabilities of failures to allow validation of dielectric strength values where they can be safely used in a field application. We have used the Weibull distribution as the analysis technique in conjunction with a computer program developed to calculate the scale and shape parameters with confidence limits for this distribution.

The experimental setup used provides a controlled test environment for the subject materials minimizing the variation in external factors and also reducing the duration of time required in duplicating and varying test conditions as desired in our investigation.

We have chosen to study thin film polymer materials namely, Polytetrafluoroethylene (PTFE) with 50  $\mu\text{m}$  thickness, Kapton with 125  $\mu\text{m}$  thickness and Nomex-Polyester-Nomex. with 150  $\mu\text{m}$  thickness, due to the increase in demand and popularity for application in industrial uses for these materials. DC voltages were applied to the test specimens and the effect of temperature on dielectric strength observed. In the case of PTFE, the temperature is raised as high as 240<sup>0</sup>C but with Kapton and Nomex-Polyester-Nomex the temperature has not exceed 160<sup>0</sup>C. 50 measurements are taken at each temperature level for the breakdown strength in increments of 20<sup>0</sup>C.



Conduction currents at high temperature and high E-fields are investigated in Kapton and Nomex-Polyester-Nomex.

A comparison is made between the dielectric strength of the subject materials. For PTFE, the dielectric strength is also investigated under application of AC voltages and compared to the results obtained with DC application.

## **ACKNOWLEDGEMENTS**

The Author would like to express his gratitude and sincere appreciation to his supervisor Dr. G. R. Govinda Raju for his advice, help and guidance through the progress of these studies. Thanks are also due to Prof. P. H. Alexander and Dr. J. B. Atkinson for their constructive comments.

He also wishes to thank Mr. Alan Johns and Mrs. Shirley A. Ouellette for their administrative help and his colleagues at KVT Technologies for their support.

Finally, his most sincere appreciation is due to his loving parents and wife for their patience, support and encouragement.

## TABLE OF CONTENTS

	Abstract	iv
	Acknowledgements	vi
	Table of Contents	vii
	List of Tables	x
	List of Illustrations	xii
Chapter 1	Introduction and Polymer Material Properties	
	1.1 Properties of Investigated Polymer Materials	1
	1.1.1 Polytetrafluoroethylene (PTFE) or Teflon	1
	1.1.2 Kapton	2
	1.1.3 Nomex-Polyester-Nomex	3
Chapter 2	Breakdown Phenomena in Polymers	
	2.1 Electrical Breakdown Phenomena	6
	2.2 Factors Determining Dielectric Strength	10
Chapter 3	Experimental Setup and Procedure	
	3.1 Experimental Apparatus	13
	3.1.1 Equipment Used for High Voltage DC and AC Tests	13
	3.2 Experimental Setup and Test Procedure for DC Voltage Application	17
	3.2.1 Experimental Setup DC Voltage	17
	3.2.2 Test Procedure DC Voltage	17
	3.3 Experimental Setup and Test Procedure for AC Voltage Application	18
	3.3.1 Experimental Setup AC Voltage	18
	3.3.2 Test Procedure AC Voltage	19
	3.3.3 Voltage Calibration	19
	3.4 Experimental Setup Advantages	21

Chapter 4	Analysis and Presentation of Statistical Techniques Employed	
	4.1 Introduction	22
	4.2 Accelerated Testing	23
	4.3 Statistical Analysis	23
	4.3.1 Statistical Method Used	23
	4.3.2 Weibull Distribution	24
	4.3.3 Graphical Technique for Estimating Weibull Parameters	26
	4.3.4 Maximum Likelihood Estimation	27
	4.3.5 Confidence intervals for Weibull Parameters	28
Chapter 5	Experimental Analysis of PTFE, Nomex-Polyester- Nomex and Kapton	
	5.1 Experimental Analysis and Results for Polytetrafluoroethylene with DC voltage application	32
	5.2 Experimental Analysis and Results for Nomex-Polyester- Nomex with DC voltage application	38
	5.3 Experimental Analysis and Results for Kapton with DC voltage application	44
	5.4 Experimental Analysis and Results for Polytetrafluoroethylene with AC voltage application	50
Chapter 6	Discussion and Conclusion	
	6.1 Breakdown induced by application of DC voltages in PTFE, Kapton and Nomex-Polyester-Nomex	56
	6.2 Breakdown induced by application of AC voltages in PTFE	60
	6.3 Electrical conduction in Kapton and Nomex-Polyester- Nomex at high fields and temperature	65
	6.4 Factors affecting accuracy of tests	65
	6.5 Suggestion for Future Work	66

Appendix I	Distribution of B/D strengths in bar chart format.	67
Appendix II	Computer Program in C++ for Calculating Parameters alpha, beta and 90% Confidence Limits	69
Bibliography		74
Vita Auctoris		76

## LIST OF TABLES

Table 1.1	Typical Property Values for PTFE and Kapton Films	4
Table 1.2	Typical Property Values for Aramid Paper (5mil Specimen, 23 <sup>0</sup> C, 50% R.H.)	5
Table 4.1	Weibull distribution equivalence w.r.t. shape parameter $\beta$	25
Table 5.1.1	Results of measurement of DC breakdown voltage in kV for 50 $\mu$ m PTFE samples	33
Table 5.1.2	Beta with 90% confidence limits for 50 $\mu$ m PTFE with DC voltage application	36
Table 5.1.3	Alpha with 90% confidence limits for 50 $\mu$ m PTFE with DC voltage application	36
Table 5.2.1	Results of measurement of breakdown voltage for 50 $\mu$ m Nomex-Polyester-Nomex samples	39
Table 5.2.2	Beta with 90% confidence limits for 150 $\mu$ m Nomex-Polyester-Nomex with DC voltage application	41
Table 5.2.3	Alpha with 90% confidence limits for 150 $\mu$ m Nomex-Polyester-Nomex with DC voltage application	41
Table 5.2.4	Conduction currents at high electric fields for 150 $\mu$ m Nomex-Polyester-Nomex	43
Table 5.3.1	Results of measurement of DC breakdown voltage for 125 $\mu$ m Kapton samples	45
Table 5.3.2	Beta with 90% confidence limits for 125 $\mu$ m Kapton with DC voltage application	47
Table 5.3.3	Alpha with 90% confidence limits for 125 $\mu$ m Kapton with DC voltage application	47
Table 5.3.4	Conduction currents at high electric fields for 125 $\mu$ m Kapton	49
Table 5.4.1	Results of measurement of AC breakdown voltage (LV) for 50 $\mu$ m PTFE samples	51

Table 5.4.2 Beta with 90% confidence limits for 50  $\mu\text{m}$  PTFE with AC voltage application 54

Table 5.4.3 Alpha with 90% confidence limits for 50  $\mu\text{m}$  PTFE with AC voltage application 54

## LIST OF ILLUSTRATIONS

Fig. 1.1	Chemical structure of PTFE	1
Fig. 1.2	Chemical structure of Kapton	2
Fig. 1.3	Chemical structure of Aramid paper	3
Fig. 2.1	Equivalent circuit of discharge in cavity	9
Fig. 3.1	Environmental Chamber	16
Fig. 3.2	Test circuit for DC setup	17
Fig. 3.3	Test circuit for AC setup	18
Fig. 3.4	Calibration graph of Transformer T2 for AC measurements	20
Fig. 4.1	Product Reliability Program Diagram	22
Fig. 4.2	Weibull Probability Distribution Function	25
Fig. 4.3	Computer Program Flowchart	31
Fig. 5.1.1	Weibull plot of DC voltage B/D of 50 $\mu\text{m}$ PTFE at 23 <sup>0</sup> C	34
Fig. 5.1.2	Weibull plot of DC voltage B/D of 50 $\mu\text{m}$ PTFE at 40 <sup>0</sup> C	34
Fig. 5.1.3	Weibull plot of DC voltage B/D of 50 $\mu\text{m}$ PTFE at 60 <sup>0</sup> C	34
Fig. 5.1.4	Weibull plot of DC voltage B/D of 50 $\mu\text{m}$ PTFE at 80 <sup>0</sup> C	34
Fig. 5.1.5	Weibull plot of DC voltage B/D of 50 $\mu\text{m}$ PTFE at 100 <sup>0</sup> C	34
Fig. 5.1.6	Weibull plot of DC voltage B/D of 50 $\mu\text{m}$ PTFE at 120 <sup>0</sup> C	34
Fig. 5.1.7	Weibull plot of DC voltage B/D of 50 $\mu\text{m}$ PTFE at 140 <sup>0</sup> C	34
Fig. 5.1.8	Weibull plot of DC voltage B/D of 50 $\mu\text{m}$ PTFE at 160 <sup>0</sup> C	34
Fig. 5.1.9	Weibull plot of DC voltage B/D of 50 $\mu\text{m}$ PTFE at 180 <sup>0</sup> C	35
Fig. 5.1.10	Weibull plot of DC voltage B/D of 50 $\mu\text{m}$ PTFE at 200 <sup>0</sup> C	35
Fig. 5.1.11	Weibull plot of DC voltage B/D of 50 $\mu\text{m}$ PTFE at 220 <sup>0</sup> C	35
Fig. 5.1.12	Weibull plot of DC voltage B/D of 50 $\mu\text{m}$ PTFE at 240 <sup>0</sup> C	35
Fig. 5.1.13	Alpha with 90% confidence limits for 50 $\mu\text{m}$ PTFE (DC voltages)	37
Fig. 5.1.14	Beta with 90% confidence limits for 50 $\mu\text{m}$ PTFE (DC voltages)	37
Fig. 5.2.1	Weibull plot of DC voltage B/D of 150 $\mu\text{m}$ Nomex-Polyester-	40



	Nomex at 23 <sup>0</sup> C	
Fig. 5.2.2	Weibull plot of DC voltage B/D of 150 $\mu$ m Nomex-Polyester-Nomex at 40 <sup>0</sup> C	40
Fig. 5.2.3	Weibull plot of DC voltage B/D of 150 $\mu$ m Nomex-Polyester-Nomex at 60 <sup>0</sup> C	40
Fig. 5.2.4	Weibull plot of DC voltage B/D of 150 $\mu$ m Nomex-Polyester-Nomex at 80 <sup>0</sup> C	40
Fig. 5.2.5	Weibull plot of DC voltage B/D of 150 $\mu$ m Nomex-Polyester-Nomex at 100 <sup>0</sup> C	40
Fig. 5.2.6	Weibull plot of DC voltage B/D of 150 $\mu$ m Nomex-Polyester-Nomex at 120 <sup>0</sup> C	40
Fig. 5.2.7	Weibull plot of DC voltage B/D of 150 $\mu$ m Nomex-Polyester-Nomex at 140 <sup>0</sup> C	40
Fig. 5.2.8	Alpha with 90% confidence limits for Nomex-Polyester-Nomex (DC voltages)	42
Fig. 5.2.9	Beta with 90% confidence limits for Nomex-Polyester-Nomex (DC voltages)	42
Fig. 5.2.10	Plot of current at 140 <sup>0</sup> C for Nomex-PolyesterpNomex at high E- fields	43
Fig. 5.3.1	Weibull plot of DC voltage B/D of 125 $\mu$ m Kapton at 23 <sup>0</sup> C	46
Fig. 5.3.2	Weibull plot of DC voltage B/D of 125 $\mu$ m Kapton at 40 <sup>0</sup> C	46
Fig. 5.3.3	Weibull plot of DC voltage B/D of 125 $\mu$ m Kapton at 60 <sup>0</sup> C	46
Fig. 5.3.4	Weibull plot of DC voltage B/D of 125 $\mu$ m Kapton at 80 <sup>0</sup> C	46
Fig. 5.3.5	Weibull plot of DC voltage B/D of 125 $\mu$ m Kapton at 100 <sup>0</sup> C	46
Fig. 5.3.6	Weibull plot of DC voltage B/D of 125 $\mu$ m Kapton at 120 <sup>0</sup> C	46
Fig. 5.3.7	Weibull plot of DC voltage B/D of 125 $\mu$ m Kapton at 140 <sup>0</sup> C	46
Fig. 5.3.8	Weibull plot of DC voltage B/D of 125 $\mu$ m Kapton at 160 <sup>0</sup> C	46
Fig. 5.3.9	Alpha with 90% confidence limits for 125 $\mu$ m Kapton (DC voltages)	48
Fig. 5.3.10	Beta with 90% confidence limits for 125 $\mu$ m Kapton (DC	48

	voltages)	
Fig. 5.3.11	Plot of current at 160 <sup>0</sup> C for 125 μm Kapton at high E- fields	49
Fig. 5.4.1	Weibull plot of AC voltage B/D of 50 μm PTFE at 23 <sup>0</sup> C	52
Fig. 5.4.2	Weibull plot of AC voltage B/D of 50 μm PTFE at 40 <sup>0</sup> C	52
Fig. 5.4.3	Weibull plot of AC voltage B/D of 50 μm PTFE at 60 <sup>0</sup> C	52
Fig. 5.4.4	Weibull plot of AC voltage B/D of 50 μm PTFE at 80 <sup>0</sup> C	52
Fig. 5.4.5	Weibull plot of AC voltage B/D of 50 μm PTFE at 100 <sup>0</sup> C	52
Fig. 5.4.6	Weibull plot of AC voltage B/D of 50 μm PTFE at 120 <sup>0</sup> C	52
Fig. 5.4.7	Weibull plot of AC voltage B/D of 50 μm PTFE at 140 <sup>0</sup> C	52
Fig. 5.4.8	Weibull plot of AC voltage B/D of 50 μm PTFE at 160 <sup>0</sup> C	52
Fig. 5.4.9	Weibull plot of AC voltage B/D of 50 μm PTFE at 180 <sup>0</sup> C	53
Fig. 5.4.10	Weibull plot of AC voltage B/D of 50 μm PTFE at 200 <sup>0</sup> C	53
Fig. 5.4.11	Weibull plot of AC voltage B/D of 50 μm PTFE at 220 <sup>0</sup> C	53
Fig. 5.4.12	Weibull plot of AC voltage B/D of 50 μm PTFE at 240 <sup>0</sup> C	53
Fig. 5.4.13	Alpha with 90% confidence limits for 50 μm PTFE (AC voltages)	55
Fig. 5.4.14	Beta with 90% confidence limits for 50 μm PTFE (AC voltages)	55
Fig. 6.1	Weibull Distribution Function for Kapton, Nomex-Polyester-Nomex and Kapton at 40 <sup>0</sup> C	57
Fig. 6.2	Weibull Distribution Function for Kapton, Nomex-Polyester-Nomex and Kapton at 120 <sup>0</sup> C	57
Fig. 6.3	Comparison of breakdown strengths (α) at DC voltages	58
Fig. 6.4	Alpha for 50 μm PTFE DC and AC voltage comparison	64
Fig. 6.5	Beta for 50 μm PTFE DC and AC voltage comparison	64
Fig. I.1	Distribution of D/C B/D strength of 50 μm PTFE at 23 <sup>0</sup> C	67
Fig. I.2	Distribution of D/C B/D strength of 150 μm Nomex-Polyester-Nomex at 120 <sup>0</sup> C	67
Fig. I.3	Distribution of D/C B/D strength of 125 μm Kapton at 60 <sup>0</sup> C	68
Fig. I.4	Distribution of A/C B/D strength of 50 μm PTFE at 240 <sup>0</sup> C	68

## CHAPTER 1

### Introduction and Polymer Material Properties

The use of insulating polymers is being promoted in many electrical devices and systems to perform many functions. Such materials are often required to retain their insulating function in the presence of moist, dirty and chemically corrosive atmospheres. They are also expected to conform to many shapes of conducting paths and are required to have suitable mechanical properties of ductility and abrasion resistances. Therefore, the study of electrical properties of insulating polymers at high temperatures has gained considerable interest due to the wide areas of application of these materials.

#### 1.1 Properties of Investigated Polymer Materials

Polymers which are stable at high temperatures and maintain good electrical properties, chemical and mechanical integrity were chosen as the subject of experimental investigation in this study. The data on general properties and range of applications for the following polymers (PTFE, Nomex-Polyester-Nomex and Kapton) has been obtained from the Handbook of Electrical and Electronic Insulating Materials [1] and other texts available on the subject of polymers. Tables 1.1 and 1.2 show physical properties for these materials.

##### 1.1.1 Polytetrafluoroethylene (PTFE) or Teflon

PTFE belongs to the family of fluoropolymers. The chemical structure of PTFE is molecularly symmetrical and it exhibits non-polar properties. It is 76% fluorine and 24% carbon by composition.

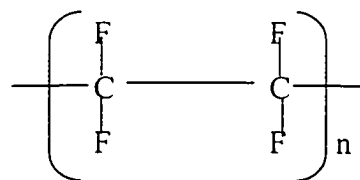


Fig. 1.1 Chemical structure of PTFE

Due to the strong carbon – fluorine bond, it has one of the widest operating temperature ranges (  $-267^{\circ}\text{C}$  to  $270^{\circ}\text{C}$  ) of all plastics. outstanding resistance to attack by chemicals. excellent dielectric properties with dielectric constant relatively unchanged with time. frequency or temperature. and virtually no tendency to absorb water.

It is widely used in military applications and has found applications in industries such as fire alarms. cables. capacitor dielectrics. motor coil. phase and ground insulation. substrate for flexible printed circuits etc.

### 1.1.2 Kapton

Kapton is an organic polyimide. It is formed as the condensation product of pyromellittic dianhydride (PMDA) with an aromatic diamine. The chemical structure of Kapton is as shown in Fig. 1.2.

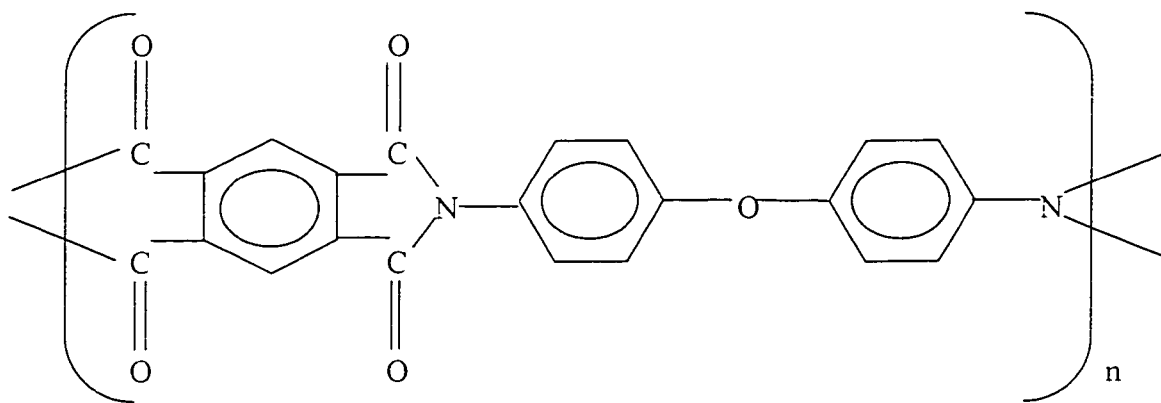


Fig. 1.2 Chemical structure of Kapton

Kapton film has no specified melting point but remains useful over a wide temperature range. It has found applications up to  $240^{\circ}\text{C}$ . Physical attributes include high tensile strength. and high resistance to creep and abrasion. Dielectric properties are generally good, although except for dielectric strength, they decrease significantly with increasing temperature. Radiation resistance and resistance to ultraviolet light are outstanding.

However, the film is vulnerable to attack by alkalis and strong inorganic acids and exhibits poor hydrophobicity.

Typical applications include use in the aircraft and space industry, motors and demanding electronic devices.

### 1.1.3 Nomex-Polyester-Nomex

Aramid paper is the generic term for a wholly aromatic polyamide paper most commonly known as Nomex. The paper has a fibrous physical structure and is used in conjunction with polyester to improve mechanical strength. The chemical structure of Aramid paper is given below:

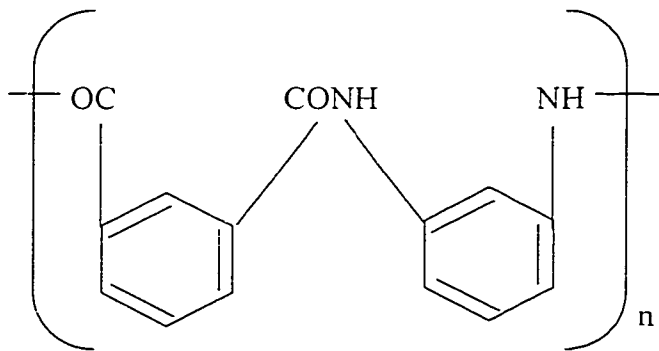


Fig. 1.3 Chemical structure of Aramid paper

Nomex-Polyester-Nomex has very high strength and tear resistance due to the laminates of polyester film but with loss in some thermal capability to about 180<sup>0</sup>C. It possesses high temperature durability (does not melt but chars), flame retardancy, excellent mechanical strength and good dielectric properties. Dielectric constant and dissipation factor increase slightly with temperatures up to 220<sup>0</sup>C. It has good resistance to acids, alkalis, refrigerants, ketones, alcohols and oils. However, it is susceptible to moisture absorption, which may improve physical properties but lowers insulating values.

Applications are found in motors, transformer insulation, cable insulation, spiral tubes and coil bobbins. It has also found uses in nuclear power plants and space applications.

Table 1.1 Typical Property Values for PTFE and Kapton Films

	PTFE	Kapton
Tensile strength, psi x 10 <sup>3</sup>	3.3	25
Elongation %	300	70
Bursting strength, 1 mil thick	-	75
Tearing strength (propagating), g/mil	10 – 100	8
Water absorption, % 24h, 1 mil thick	Nil	2.9
Water vapor transmission rate, g/100 sq in 24h @ 38 <sup>o</sup> C, 90% R.H.	-	5.4
Permeability to gases cm <sup>3</sup> /100 sq in 24h. @ atmospheric pressure, 23 <sup>o</sup> C, 0% R.H.		
O <sub>2</sub>	-	25
CO <sub>2</sub>	-	45
Dielectric strength, volts/mil, short time 50% R.H., 23 <sup>o</sup> C, 1 mil* film	2,200 – 4,400	7,000
Dielectric constant @ 23 <sup>o</sup> C		
10 <sup>3</sup> cycles	2.0	3.5
10 <sup>6</sup> cycles	2.0	3.4
Dissipation factor @ 23 <sup>o</sup> C		
10 <sup>3</sup> cycles	0.0001	0.0025
10 <sup>6</sup> cycles	0.0001	0.010
Volume resistivity, Ω cm, 23 <sup>o</sup> C	10 <sup>18</sup>	10 <sup>18</sup>
Chemical resistance (G=good, F=fair, P=poor)		
Strong acids	G	G
Strong alkalies	G	P
Greases and oils	G	G
Organic solvents	G	G
Maximum use temperature, <sup>o</sup> C	260	240
Thickness range, mils		
Minimum	0.25	0.3
Maximum	30	5
Maximum available width, inches	48	60
Specific gravity	2.1	1.4

\* 1 mil = 0.001 inch.

Table 1.2 Typical Property Values for Aramid Paper (5 mil Specimen, 23<sup>0</sup>C, 50% R.H.)

	Aramid Paper
Tensile strength, lb/in	
Machine direction	80
Transverse direction	40
Elongation %	
Machine direction	16
Transverse direction	13
Elmendorf tear, grams	
Machine direction	240
Transverse direction	520
Dielectric strength ac rapid rise V/mil	635
Dielectric constant, 60 Hz, 23 <sup>0</sup> C, 50% R.H.	2.4
Dissipation factor, 60 Hz, 23 <sup>0</sup> C, 50% R.H.	0.006
Chemical resistance (G=good, F=fair, P=poor)	
Strong acids	G
Strong alkalies	G
Greases and oils	G
Organic solvents	G
Maximum use temperature, <sup>0</sup> C	220

## CHAPTER 2

### Breakdown in Polymers

While there is considerable literature available on the breakdown phenomena in published texts, this chapter serves as an overview of some factors in brief which influence dielectric strength of polymers and the processes involved leading to breakdown. The magnitude of the electric field at which dielectric breakdown occurs in an insulating material is defined as the dielectric strength (V/m) of that material [2]. Breakdown occurs when the applied voltage can no longer be maintained across the polymer without excessive flow of current and change of its physical properties.

#### 2.1 Electrical Breakdown Phenomena

Many attempts have been made to provide theories of dielectric breakdown that apply to different experimental conditions with polymers. We propose to set out the assumptions underlying the various types of acknowledged theories in an attempt to understand what role they may play in this specific study, the most recognized of which are: intrinsic breakdown, thermal break down, discharge dependent breakdown and electromechanical breakdown. Conditions and material characteristics determine the type of breakdown and can be a combination of two or more types simultaneously or sequentially.

**Intrinsic Breakdown:** The intrinsic breakdown of the solid is defined by the characteristics of the material itself in pure and defect free form under test conditions which produce breakdown at the highest possible voltage. It is assumed valid for limiting values of electric field at very short times and very thin specimens at lower temperatures. In this type of breakdown the field causes either the number or the energy of the electrons to reach unstable magnitudes such that they rise catastrophically resulting in dielectric failure. The power balance equation which can only be satisfied below a critical value of field or voltage, relates to the rate of gain and loss of electron energy. Free electrons on average gain energy from the field at a rate:

$$A = JE / n, \quad (2.1)$$



where  $A$  is the energy gained by free electrons from the field,  $J$  the current density,  $n$  the charge carrier number density, and  $E$  the electric field strength.

In this equation both  $J$  and  $n$  may depend on temperature,  $T$ , and other parameters,  $\partial$ , describing the electron energy bands, trap levels etc.

The rate of energy loss is unlikely to be explicitly dependent upon field except in as much as it may result in heating. The electron power loss  $B(T,\partial)$  at equilibrium is therefore defined by

$$A(E,T,\partial) = B(T,\partial) \quad (2.2)$$

Various models have been developed by von Hippel and Frohlich [12] based on (2.2). These models differ from each other by considering different mechanisms of energy transfer from the conduction electrons to the lattice, and also by the different assumptions they make considering the energy distribution of the conduction electrons. It is also of interest to note that the general experimental conditions under which intrinsic breakdown should occur, requires that the electric current cause a negligible rise in the lattice temperature. This condition is strongly fulfilled in materials with a low ratio of electrical to thermal conductivity.

**Thermal Breakdown:** When an electric field is applied to a solid dielectric there are always some currents which generate heat. Conduction currents from ionic dissociation, currents due to ionic or dipolar changes not involving transport of charged particles to electrodes, generate heat in an alternating field because these changes have a finite relaxation time which is evidence of dissipation in a system. These currents also known as 'loss currents' are much greater in alternating than in constant fields because the energy loss in relaxation phenomena such as dipolar motions, the most important in solid dielectrics, depends upon the rate of change of field strength. The energy loss increases with the field strength, and if high enough the dielectric specimen may be unable to dissipate the heat from the regions where it is generated. The temperature rises and breakdown ensues because the intrinsic electric strength falls ultimately with increase of temperature, and finally the dielectric decomposes.

The theories of intrinsic breakdown do not consider the sources of electric field. However, in the case of thermal breakdown the electrode geometry is often of prime importance. Against this, much of the investigative work on thermal breakdown is done with arrangements that allow a uniform distribution of field in the most intense part, such as sphere plane electrodes.

The fundamental equation of thermal breakdown based on thermal conduction as the only significant loss process in lattice energy is given by:

$$C_v \frac{dT}{dt} - \text{div}(k \text{ grad}T) = \sigma E^2 \quad (2.3)$$

where,  $C_v$  is the specific heat per volume,  $k$  is the thermal conductivity,  $dT/dt$  is the time derivative of temperature,  $\text{grad}T$  the space gradient of temperature,  $\sigma$  the electrical conductivity and  $E$  the electric field strength. Since  $\sigma$  and  $k$  are strongly temperature dependent, even approximate analytic solutions of (2.3) are not possible for any, but the simplest boundary conditions. A detailed treatment of thermal breakdown and typical solutions is provided by Whitehead [17]. The principal result is that there exists a critical field strength  $F_c$  for which the temperature of the hottest part of the dielectric asymptotically approached some temperature  $T_c$  with time. For field strengths greater than  $F_c$  the temperature reaches the value  $T_c$  in a finite time and thereafter increases without limit, while for lower field strengths the temperature rises slowly to some upper limit which depends on the field strength.

**Discharge Dependant Breakdown:** Small voids inevitably occur in polymers even in carefully prepared materials. Since these are filled with gas they have a lower permittivity than the surrounding polymer and so field intensification occurs at the end walls in the direction of the local field. Depending on the gas pressure and other factors the enhanced field may cause the gas to become ionized and cause discharge which results in degradation over time and result in breakdown in the polymer. The carriers produced by the ionization are accelerated across the void and, if they acquire sufficient energy from the field they can cause erosion as they impact on the opposite wall of the void. In thin films this may quickly lead to failure, whereas, in thick specimens in which larger voids are more likely to occur but less likely to be detected, these partial discharges produce

electrical trees which act as degradation mechanisms with breakdown not occurring immediately. Here breakdown occurs eventually over a period of time.

The precise conditions under which partial discharges can be initiated will depend upon a variety of factors such as the gaseous content, gas pressure, void shape and size of void. We can model the equivalent circuit of a void in the dielectric as an analogue circuit. For the simple case of disc shape dielectric, the equivalent circuit can be represented as

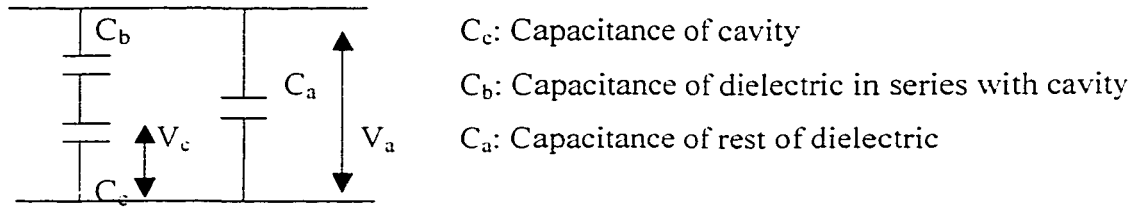


Fig. 2.1 Equivalent circuit of discharge in cavity

The voltage across the cavity is

$$V_c = C_b V_a / (C_c + C_b) = V_a / (1 + (1/\epsilon_r) (d/t - 1)) \quad (2.4)$$

where  $\epsilon_r$  is the relative permittivity of the dielectric,  $d$  is the thickness of the dielectric and  $t$  is the thickness of the cavity.

Assuming that the gas filled cavity breakdown stress is  $E_{cb}$ , the voltage across the dielectric which will initiate discharge in the cavity (inception voltage) is given by

$$V_i = E_{cb} t (1 + (1/\epsilon_r) (d/t - 1)) \quad (2.5)$$

If the voltage applied exceeds the inception voltage then the void is likely to discharge until its voltage drops to below the extinction voltage. The nature of the discharge and the criterion for a self sustaining discharge has been developed by Townsend using classical theories and Paschen's law [21]. The Townsend discharge is based on electrons injected from the cathode which gain energy from the field causing an initial avalanche which causes secondary avalanches thus making the current self sustaining and resulting in ultimate breakdown.

**Electromechanical Breakdown:** Substances which can deform appreciably without fracture may collapse when the electrostatic compression forces on the test specimen exceed its mechanical compressive strength. The compression forces arise from the electrostatic attraction between surface charges which appear when voltage is applied. In the Stark and Garton mechanism [11], if  $d_0$  is the initial thickness of a specimen of material of Young's modulus  $Y$ , which decreases to a thickness of  $d(m)$  under an applied voltage  $V$ , then the electrically developed compressive stress is in equilibrium with the mechanical compressive strength if

$$\epsilon_0 \epsilon_r V^2 / 2d^2 = Y \ln (d_0 / d) \quad (2.6)$$

or  $V^2 = d^2 ( 2Y / \epsilon_0 \epsilon_r ) \ln (d_0 / d)$

where  $\epsilon_0$  and  $\epsilon_r$  are the permittivity of free space and the relative permittivity of the dielectric. Differentiating with respect to  $d$  the expression (2.6) has a maximum when  $d / d_0 = \exp(-0.5) = 0.6$ . Therefore, no real value of  $V$  can produce a stable value of  $d / d_0$  less than 0.6. If the intrinsic strength is not reached at this value, a further increase in  $V$  makes the thickness unstable and the specimen collapses. The highest apparent strength is then given by

$$E_a = V / d_0 = 0.6 ( Y / \epsilon_0 \epsilon_r )^{1/2} \quad (2.7)$$

This treatment ignores the possibility of instability occurring in lower average field because of stress concentration at irregularities, the dependence of  $Y$  on time and stress, and also on plastic flow.

## 2.2 Factors Determining The Dielectric Strength

The dielectric strength of a polymer is affected by several principal factors depending on the application and environmental condition of the specimen. The intrinsic dielectric strength of a polymer is rarely realized in practice due to the fact that these external factors lower the breakdown voltage. One or a combination of these factors may dominate and influence the physical and chemical property of the material leading to

degradation and lowering of breakdown strength. The factors are described in brief below.

**Environmental Conditions:** Environmental conditions such as exposure to oxidation, ozone, radiation and chemicals cause chemical bonds within the polymer to weaken and break. Often the chemical structure of the base material is affected leading to a change in material properties and thus weakening the dielectric strength. Moisture introduces a conductive path ( or treeing ) within hygroscopic polymers lowering the dielectric strength of the material and leading to premature failure. For polymers with good hydrophobicity, conductive paths can be formed on the surface and with the presence of contaminants the breakdown process is accelerated.

**Specimen Thickness and Conditioning:** The dielectric strength for a given material is considered to be significantly greater per unit thickness for thin than for thick specimens of the same material. This is explained by the fact that with increased thickness, more dielectrically weaker paths are available, the weakest of which causes breakdown. Physical defects such as voids and contaminants present within a polymer specimen provide locations for initiation of destructive action by electrical discharge (partial discharge or corona effect), moisture and contaminant reaction leading to degradation which lower the breakdown strength.

**Electrode effects:** The properties of the electrode system influences the breakdown strength depending on the temperature region under consideration. It has been experimentally confirmed that different metallic electrode materials yield slightly different breakdown strengths, but that use of an electrolytic solution as a cathode produces markedly different results from that obtained with a metallic cathode. Size and geometry of electrodes also affect the dielectric strength. The larger the area of the electrodes, the lower the value of dielectric strength. Depending on the configuration of the electrodes, the voltage gradient present may be non-uniform forcing the electrical stress to concentrate in a specific region, such as on the edges of the electrode, forming

creepage paths which can cause volume breakdown. Therefore, it is important to consider the geometry on voltage breakdown when conducting tests.

**Method of Voltage application:** Another factor affecting the dielectric strength value is the rate of voltage rise and whether it is continuous or step by step. A slow rate of increase usually encourages time dependant thermal degradation due to local heating, resulting in lower dielectric strength values, whereas a rapid application of voltage promotes electronic conduction providing values closer to that which is achieved by intrinsic breakdown.

**Temperature:** Temperature affects the intrinsic, thermal and discharge initiated voltage breakdown strength of most polymers. Non-polar polymers maintain relatively constant and low electric breakdown strength at low temperatures but the breakdown strength increases with decreasing temperature for polar polymers. High temperatures can cause deformation of the physical structure of the specimen and increase oxidation and corona effects. Aqueous and electrical treeing are also accelerated causing tracking and degrading the electrical properties of the material.

**Frequency:** The heat generated in a dielectric is directly proportional to the frequency applied. Therefore, high frequencies lead to thermal degradation thus lowering the dielectric strength value. At high frequencies breakdown depends largely on the geometry and arrangement of electrodes and the surrounding environment and less on the material.

## CHAPTER 3

### Experimental Setup and Procedure

Experience has shown that the thermal life characteristics of a polymer composite insulating system cannot be reliably inferred solely from characteristic information of the polymer material. To assume satisfactory service life, insulation specifications need to be supported by service experience or life tests. These are usually lengthy and complicated and prone to variation in external factors, which can directly affect results. Therefore, in order to overcome these problems, the method of accelerated life tests may be used to evaluate the insulating properties of polymer materials, shortening the period of service experience required before they can be used with confidence. The experimental setup used by the author in this study simulates conditions of service for insulating polymers, which are complex and lengthy. The setup used provides the advantage of a simple equipment arrangement with ease of duplicating necessary conditions for repeatability of tests efficiently.

#### 3.1 Experimental Apparatus

The experimental arrangement consists of DC and AC voltage generators, an environmental chamber and multimeters to measure voltage and indicate breakdown occurrence with following specifications. The setup was arranged to experiment with DC and AC voltages on thin films of polymers as follows:

##### 3.1.1 Equipment Used for High Voltage DC and AC Tests

###### High Voltage DC Generator

Type Brandenburg model # 2807R

Voltage range: 0 kV to 30 kV at 1mA.

### **High Voltage Voltmeter (DC)**

Type Direct reading Brandenburg digital meter model 139D

Measurement range: 0 kV to 40 kV

Resolution = 10 V at 20 kV and 100 V at 40 kV.

### **High Voltage AC Generator**

High voltage AC generator consists of three elements for production of high voltage consisting of:

Vac: Low voltage source 120 V (City Line).

T1: VARIAC (Autotransformer)

Make: General Radio Company

Ratings: Input 120 V, 5A

Output variable from 0 V to 130 V.

T2: Step-up Transformer (type luminous tube)

Ratings: Primary 120 V, 60 Hz, 270 VA

Secondary 9 kV, 30 mA (Secondary midpoint grounded)

### **Voltmeter and Ammeter (LV)**

Philips Multi meter, Accuracy class 3, and BIL 3 kV.

AC measurements are rms values and are converted to peak values in this study.

### **Environmental chamber**

An oven is used as an environmental chamber to simulate service conditions. Design features include a 12" x 12" casing of 16 Gauge galvanized steel and a hinged door with



a tempered glass window for observation. Thermal insulation of ceramic fiber is present on the inner walls to prevent heat loss. A heater element is situated within the chamber to provide heat. Temperature control is achieved by a digital PID controller including a thermocouple as a sensing element. Two electrodes of 1/8" steel with ceramic insulation are present inside and extend to the outside of the chamber for connection to a voltage source. The bottom electrode is fixed whereas the upper electrode is movable vertically from the outside using a knob link mechanism. The electrodes are circular-planar, the upper 3/4" diameter and the lower 2" diameter. The test sample roll is fed from a spool mounted on the inside of the chamber wall on one side and passed through a thin opening on the other side of the chamber wall to a returning spool. The material is passed between the electrodes from one spool to the other. Once a sample is tested, the film roll is retracted with the retracting spool and a new part of the sample is introduced under the electrodes. This provides the advantage of speeding up sample replacement without affecting service conditions. See Fig.3.1.

### **Temperature Calibration**

To improve the accuracy of temperature measurement, a JK thermocouple meter is connected on the inside of the chamber and temperature settings confirmed using the readings from the meter. The PID temperature controller is adjusted until the required temperature is reached and confirmed by the thermocouple meter.

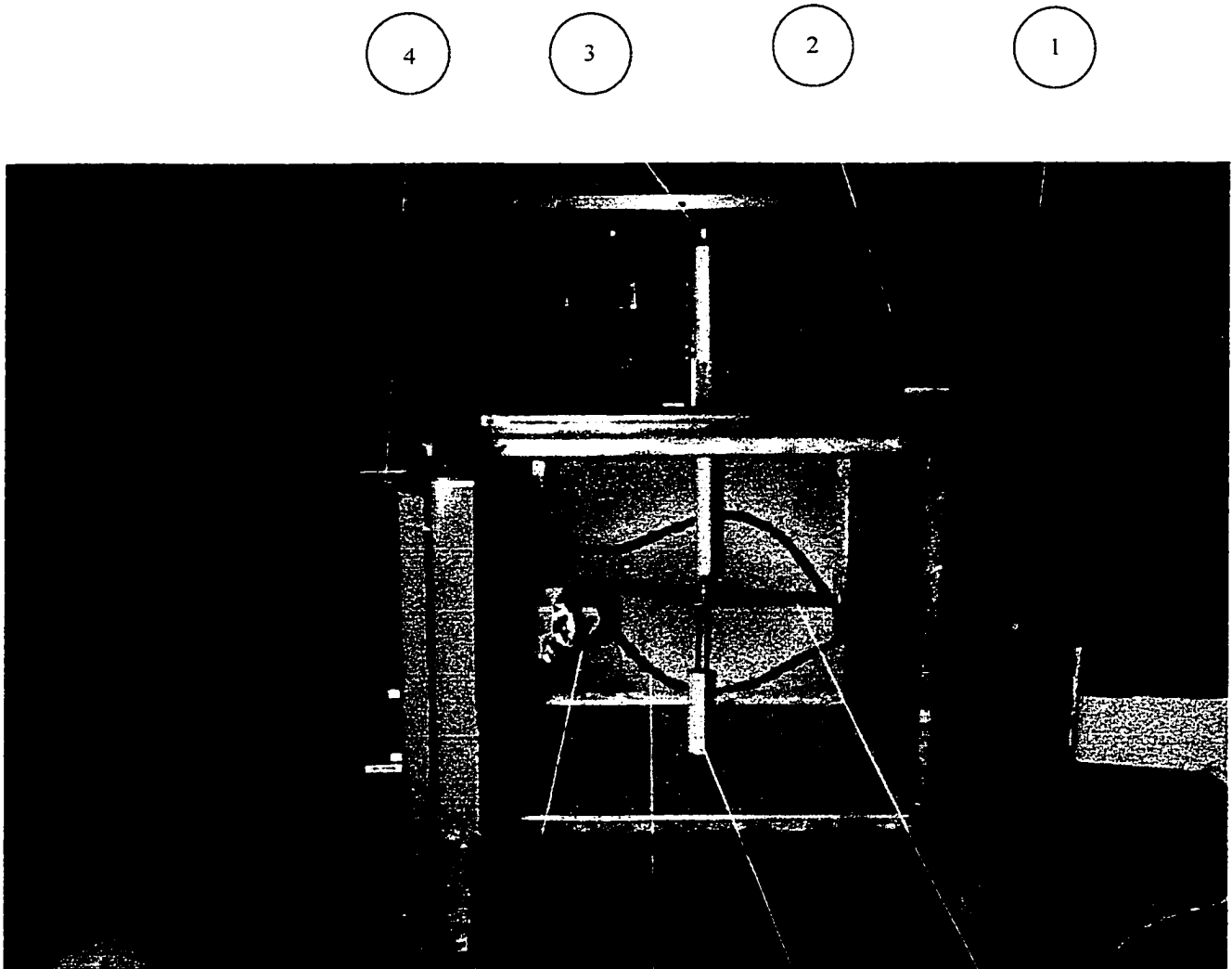


Fig. 3.1 Environmental Chamber



1. Retracting Spool 2. Knob for Raising and Lowering Upper Electrode  
 3. Upper Electrode 4. PID Temperature Controller 5. Test Specimen Roll  
 6. Lower Electrode 7. Heating Element 8. Feeding Spool

## 3.2 Experimental Setup and Test Procedure for DC Voltage Application

### 3.2.1 Experimental Setup DC Voltage

The test circuit setup for DC voltage tests is as follows:

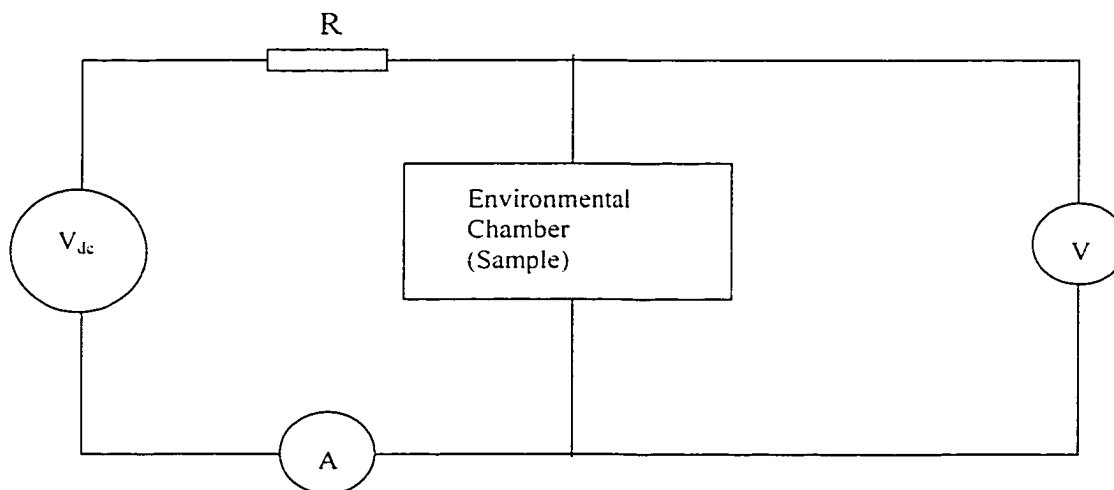


Fig. 3.2 Test circuit for DC setup.

where,

$V_{dc}$ : High Voltage DC generator

$V$ : High Voltage Voltmeter

$R$ : Current Limiting Resistor

$A$ : Ammeter

### 3.2.2 Test Procedure DC Voltage

The test materials used are in the form of film rolls which are cut to approximately 3" in width and wound over the feeding spools of the environmental chamber. The film is passed between the electrodes from the feeding spool on one side to a retracting spool on the other via a thin opening on the side of the chamber. After passing the film between the electrodes, the top electrode is lowered using the knob mechanism and the film is trapped securely between the electrodes.

The chamber door is closed and the heater is turned on. Once thermal equilibrium is reached inside the chamber, tests and measurements can be conducted. In order to support the Weibull analysis method, voltage should be applied increasingly either in steps or gradually to the electrodes. In our case, we increase the voltage gradually until breakdown is achieved. Breakdown is observed when the voltage across the sample suddenly drops and current begins to flow through the ammeter. The current limiting resistor protects from excessive dangerous currents or short circuit situations. The last reading observed on the high voltage voltmeter just before breakdown is taken as the breakdown value for that test. After breakdown the sample is punctured especially in the case of the thinner specimens of polymers tested. The upper electrode is raised using the knob and the tested portion of the sample film is cleared using the retracting spool. A new portion of the sample is now introduced between the electrodes, the top electrode is lowered again and the test is repeated on the new sample of material at the same temperature. In this study we conduct 50 tests at each temperature level.

### 3.3 Experimental Setup and Test Procedure for AC Voltage Application

#### 3.3.1 Experimental Setup AC Voltage

The test circuit setup for AC voltage tests is as follows:

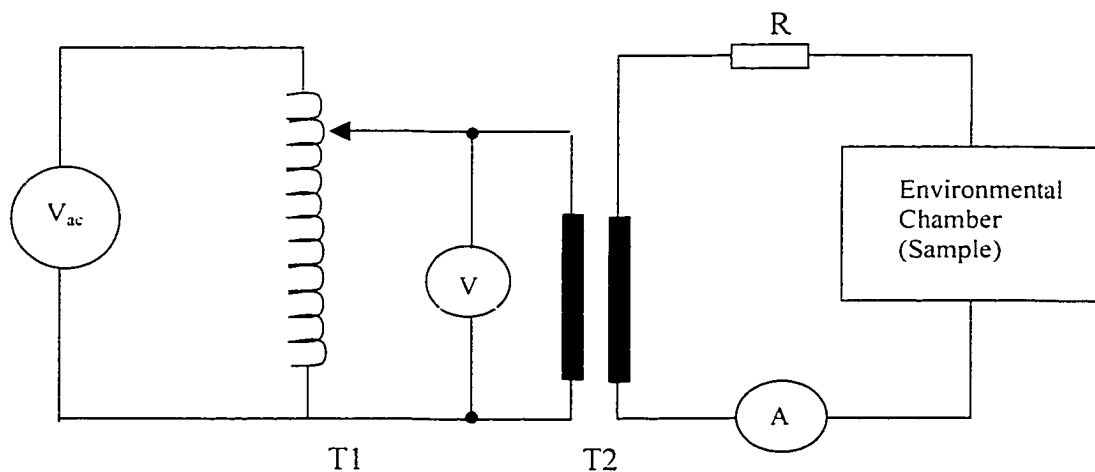


Fig. 3.3 Test Circuit for AC Setup.

where,

Vac: Line voltage 120V

T1: VARIAC

T2: Step-up Transformer

R: Current Limiting Resistor

A: Ammeter

V: Voltmeter

### **3.3.2 Test Procedure AC Voltage**

Test procedure is similar to that applied for DC voltages. However, in order to generate high voltage the items described in 3.1.1 are setup as shown in figure 3.3. The voltage on the low voltage side is varied using T1, stepped up by T2 and applied to the electrodes of the environmental chamber. Measurements are made on the low voltage section of the circuit and converted to a high voltage result using a calibration graph (see 3.3.3).

### **3.3.3 Voltage Calibration**

Calibration of the output voltage of transformer T2 is obtained from the graph in Fig.3.4. A varying input voltage is applied using the variac on the low voltage side (measured by the voltmeter) and the corresponding output voltage measured by a high voltage vacuum meter at the output of transformer T2. Output voltage during testing is obtained by measuring the voltage in the low voltage section of the circuit and converting it to the corresponding value using the calibration graph.

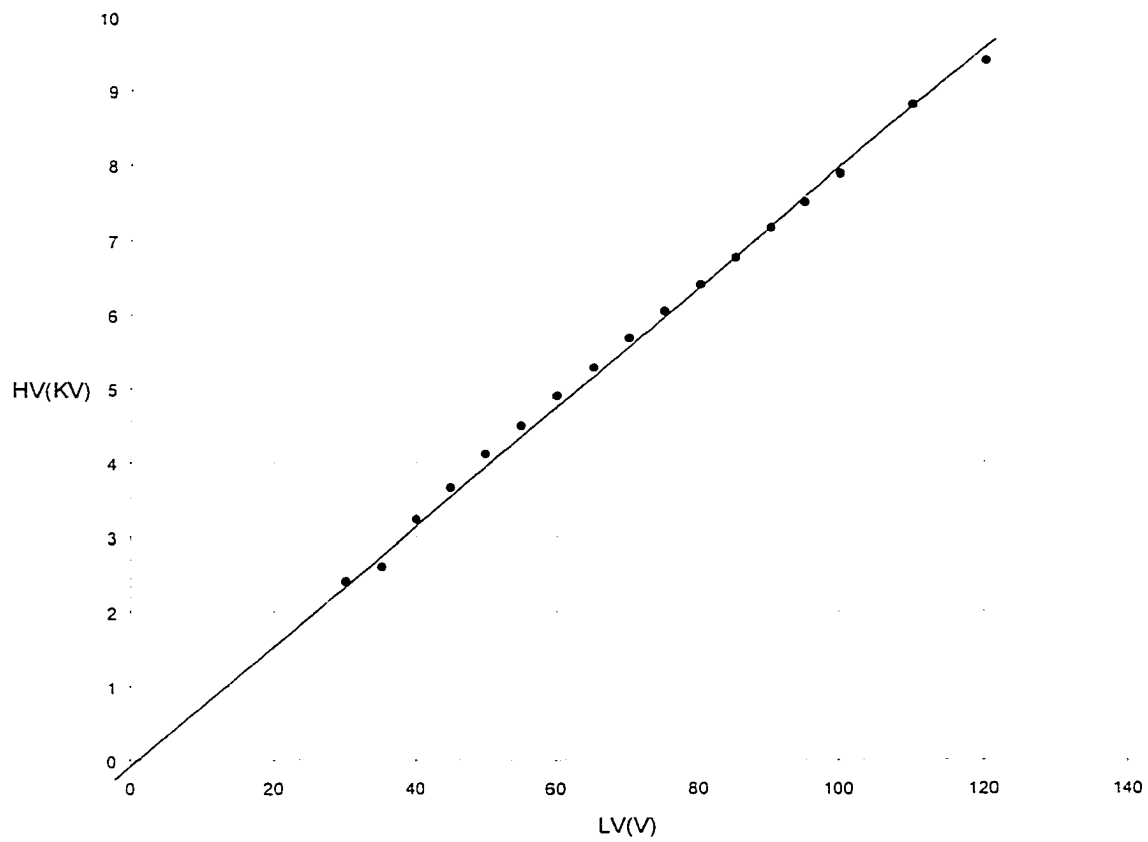


Fig 3.4 Calibration Graph of Transformer T2 for AC Measurements

LV: Voltage of primary winding of T2

HV: Voltage of secondary winding of T2

### **3.4 Experimental Setup Advantages**

The above setup offers several advantages during testing, some of which are listed below:

#### **Same Sample History of Material under Investigation**

- Same batch samples can be assumed to have the same manufacturing history, handling, storing and test preparation conditions
- Speed of tests allow negligible difference in conditions from beginning to end of ribbon

#### **Negligible Temperature Difference across the Sample**

- Thin area of test samples under electrical stress allows little temperature variation across the sample, although temperature difference may vary in the depth of chamber.

#### **Small Time Differences between Consecutive Tests**

- After thermal equilibrium, tests can be conducted very rapidly; limiting factor is sample refreshing time (couple of seconds)
- Because of reduced test duration, an increased number of test points can be applied for better statistical analysis.

#### **Time to Equilibrium and Temperature Accuracy**

- Usually 1 hour.
- Additional thermocouple provides increased accuracy of temperature measurement and control.

## CHAPTER 4

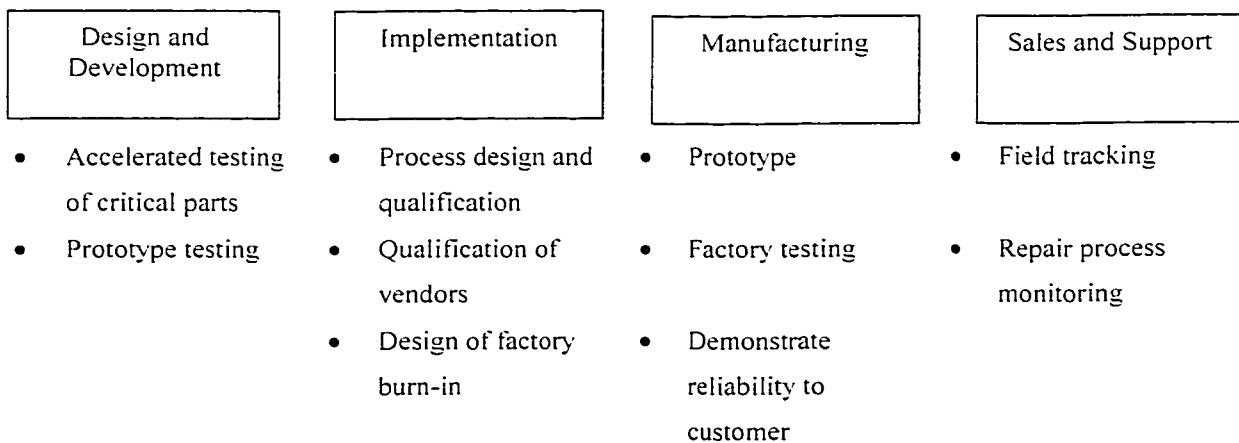
### Analysis and Presentation of Statistical Techniques Employed

#### 4.1 Introduction

Statistical methods for the analysis and presentation of reliable life data play an important role in the design and manufacture of reliable products. The methods are an essential part of the accelerated life testing of critical parts, prototype testing, process design and qualification, prototype and field tracking studies.

A product reliability program helps to ensure that the delivered product meets or exceeds its reliability objectives, and does so economically. Such a program is comprised of a coordinated set of activities that begin at the early stages of item design and continue through to design and development, implementation, manufacturing, and sales and support [3]. Fig. 4.1 shows some reliability program activities that involve statistical methods for analyzing and presenting reliability data.

Fig. 4.1 Product Reliability Program Diagram



Of the above activities, the preliminary and one of the most important is accelerated testing of critical parts. Data achieved from this is vital in determining and substantiating whether the specimen under test will conform to application requirements.



## **4.2 Accelerated Testing**

The method of accelerated life testing is used to test items at higher than normal stress in order to speed up time and induce early failures. The advantages of this procedure are quicker results and increased precision in the estimates of population parameters when the test time and sample size are constrained. Accelerated life tests are based on the physical assumption that all failure mechanisms are affected by accelerating stress in the same way. This assumption is approximately correct when there is a single or predominant failure mechanism. This assumption is upheld in our study as the test is performed by steadily increasing the voltage, ultimately resulting in electrical breakdown.

## **4.3 Statistical Analysis**

### **4.3.1 Statistical Method Used**

Numerous parametric models are used in the analysis of lifetime data and in problems related to modeling of aging or failure processes. Among the univariate models used, the exponential, Weibull, gamma, and log-normal distributions have demonstrated usefulness in a wide range of situations [4]. Of these models, the Weibull distribution is perhaps the most widely used lifetime distribution model. Its application in connection with lifetimes of many types of manufactured items has been widely advocated and has been used as a model with diverse types of items such as vacuum tubes and electrical insulation [5]. This study focuses on using the Weibull model in analyzing the electrical breakdown characteristics of different polymers.

### 4.3.2 Weibull Distribution

The cumulative Weibull distribution function [6] is given by:

$$F(t) = 1 - \exp [ - ( \{t - \gamma\} / \alpha )^\beta ] \quad (4.1)$$

Where,

$\alpha$  is the scale parameter

$\beta$  the shape parameter

$\gamma$  the location parameter

$t$  the random variable, usually time to breakdown or breakdown strength

Using the above function we convert the Weibull distribution function to analyze failure probabilities using E field or voltage instead of t as the random variable. This holds since the voltage is increased at a constant rate until the dielectric is punctured in our case. Substituting E as the random variable in the above equation we get

$$P_F(E) = 1 - \exp [ - ( \{E - \gamma\} / \alpha )^\beta ] \quad (4.2)$$

Here

- E is the electric field (random variable), V/m
- $P_F(E)$  indicates the probability specimens tested will fail by magnitude E
- $\alpha$  represents the magnitude of E required for  $(1 - e^{-1})$  or 63.2% of tested units to fail (V/m)
- $\beta$  is a measure of dispersion of failure magnitude E from  $E = \alpha$ . If  $\beta > 1$ , dielectric fails because of wear, if  $\beta < 1$  failure due to irrelevant mechanism
- $\gamma$  is that value of E field before which breakdown is not possible and is also referred to as the threshold parameter (V/m)

Both  $\alpha$  and  $\beta$  are properties of the dielectric. The shape of the Weibull probability distribution function depends upon the value of  $\beta$ . Typical  $\beta$  values vary from application to application, but in many situations distributions with  $\beta$  in the range 1 to 4 seem

appropriate. Fig. 4.2 shows some Weibull probability distribution functions for  $\alpha = 1$  and several different values of  $\beta$ .

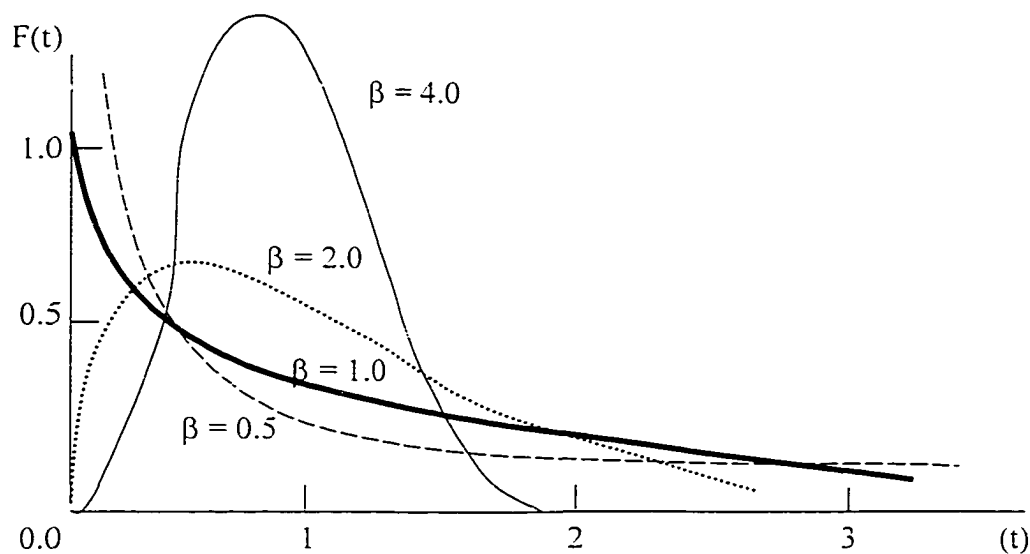


Fig. 4.2 Weibull Probability Distribution Function for  $\beta = 0.5, 1.0, 2.0$  and  $4.0$  with  $\alpha = 1$

The shape parameter  $\beta$  indicates that for different values, the Weibull distribution tends to the following equivalent distributions:

Shape Parameter ( $\beta$ )	Equivalent Distribution
$\beta = 1$	Exponential
$\beta = 2$	Lognormal
$\beta = 4$	Gaussian

Table 4.1 Weibull distribution equivalence with respect to shape parameter  $\beta$

Since  $\alpha$  is the scale parameter, the effect of different values of  $\alpha$  is just to change the scale on the horizontal axis, and not the basic shape of the graph. It determines the spread of values. The parameter  $\beta$  determines shape and spread of the distribution; when  $\beta$  is greater than 1, the hazard rate increases with time (unbounded); when it is less than 1, it decreases (to zero); and when it equals 1, the exponential distribution is obtained with its constant hazard rate [3]. An interpretation of the shape parameters indicates that if  $\beta$  is greater than 1, the dielectric progressively deteriorates leading ultimately to breakdown.

If  $\beta$  is less than 1, which is uncommon, the dielectric failure rate decreases with time because of a decreasing hazard function. It indicates a conditioning process in which the system is less at risk in each successive time interval and suggests that pre-breakdown events, each of which may separately lead to breakdown, retard one another's subsequent generation and development.

To obtain values for the above parameters we will utilize two methods for estimation of these parameters for the dielectric strength in our investigations.

#### 4.3.3 Graphical technique for estimating Weibull parameters

This method involves the use of Weibull probability paper. The time (or voltage axis) and the cumulative probability axis are scaled so that the data drawn from a Weibull distribution, will appear as a straight line. To use the Weibull plot, the failure times or voltages are first ordered from smallest to largest.

It has been shown by Fothergill [7] that the cumulative probability of failure for the  $i^{\text{th}}$  of  $n$  identically stressed samples, the following approximation is considerably more accurate than other commonly used approximations

$$F(i,n) = (i - 0.3) / (n + 0.4) \quad (4.3)$$

Thus the first failure has the lowest probability and last failure has the highest which is not equal to 1. The equation is a good formula for calculating  $P_F(E)$ . The data is plotted on the probability paper  $\text{Ln} [ \text{Ln} (1/(1 - P_F(E))) ]$  vs  $\text{Ln}(E)$  [8] and a straight line fitted arbitrarily by eye or by performing a least square analysis to determine  $\alpha$  and  $\beta$ .

The parameters  $\alpha$  and  $\beta$  are calculated as follows:

$\alpha$  is taken as that value of voltage corresponding to  $P_F(E) = 63.2\%$

$\beta$  is estimated with  $\gamma = 0$  from :

$$\beta = \frac{\{ \text{Ln} [ \text{Ln} (1/(1 - P_F(E_1))) ] - \text{Ln} [ \text{Ln} (1/(1 - P_F(E_2))) ] \}}{\text{Ln} (E_1/E_2)} \quad (4.4)$$

where  $(E_1, 1/(1 - P_F(E_1)))$  and  $(E_2, 1/(1 - P_F(E_2)))$  are two points on the fitted straight line.

For  $\gamma \neq 0$ : an estimate of  $\gamma$  can be found graphically by a trial and error process where a guessed value of  $\gamma'$  is subtracted from each individual experimental failure value (B/D strength) and repeated until a sound straight line is achieved

The method of graphical estimation has certain limitations. It is observer dependent and is strictly not valid for censored data. Censoring involves termination of a test on  $n$  samples before all samples fail. Two common types of censoring are commonly utilized, namely Type I and Type II. Type I censoring involves termination of test at a predetermined voltage or time. In Type II censoring, the test is terminated after the first  $r$  failures in a sample of  $n$  items, irrespective of voltage or time. In this study, however, the tests were conducted on all samples to failure and censoring was not involved. In the Weibull plot, a small change in fitted line will result in great changes in  $\alpha$  and  $\beta$ , especially  $\beta$  because of the double exponential characteristic. However, the most serious limitation here is that confidence intervals for  $\alpha$  and  $\beta$  cannot be derived. Therefore, a different technique, which is the method of maximum likelihood estimation is applied in such a situation where confidence limits can be defined and thus provide more useful presentation of data for interpretation.

#### 4.3.4 Maximum Likelihood Estimation

The Maximum likelihood theory is a well known statistical technique which is used to obtain estimates of parameters for probability distributions. To apply this theory, a likelihood function is generated for the Weibull distribution. This likelihood function is then maximized with respect to the parameters of interest by setting its first derivatives to zero. The resulting equations will allow determination of the best estimates of the parameters from experimental data. When applied to the Weibull distribution [9], this technique yields the following formula for  $\alpha$  and  $\beta$  for  $n$  uncensored samples

$$f(\beta) = A_2/A_1 - 1/\beta - C = 0 \quad (4.5)$$

$$\text{and } \alpha = (A_1 / n)^{1/\beta} \quad (4.6)$$

$$\text{where } A_k = \sum_{i=1}^n E_i^\beta [\ln E_i]^{(k-1)} \quad (4.7)$$

for  $k = 1, 2, 3, \dots, n$

$$\text{and } C = 1/n \sum_{i=1}^n \ln E_i \quad (4.8)$$

where  $E_i$  is the failure voltage of the  $i^{\text{th}}$  unit tested.

Equation (4.5) is in terms of  $\beta$  only and can be solved by the Newton Raphson iterative technique

$$\beta_{j-1} = \beta_j - f(\beta_j) / f'(\beta_j) \quad (4.9)$$

where

$$f'(\beta) = A_3/A_1 - (A_2/A_1)^2 + 1/\beta^2 \quad (4.10)$$

$\alpha$  is then calculated from  $\beta$ .

#### 4.3.5 Confidence Intervals for Weibull Paramters

Repetition of the same experiment consisting of  $n$  number of voltage applications several times will produce different values of  $\alpha$  and  $\beta$  for the same specimen.  $\alpha$  and  $\beta$  calculated from the results will unlikely be the true values of  $\alpha$  and  $\beta$  if the experiment was carried out with an infinite number of specimens. Therefore, intervals are formed for parameters to determine with a high degree of confidence that the true values of  $\alpha$  and  $\beta$  are within the given intervals if experiments are repeated a sufficient number of times. These are defined as the confidence intervals. Confidence intervals are available from tables [10] with limitations on sample size or from a numerical approximation. In this study we use a numerical approximation as follows:

### Numerical Approximation for $\beta$ [11]

Accuracy within 1 % for  $n < 120$

Approximations as follows:

$$\beta_u = \beta \times [ u_0 + u_1.n + u_2.n^2 + u_3.n^3 + u_4.n^4 ] \quad (4.11)$$

where

$$u_0 = 1.63617$$

$$u_1 = -0.0272229$$

$$u_2 = 5.78997 \times 10^{-4}$$

$$u_3 = -5.39819 \times 10^{-6}$$

$$u_4 = 1.80269 \times 10^{-8}$$

and

$$\beta_l = \beta / [ l_0 + l_1/n + l_2/n^2 + l_3/n^3 ] \quad (4.12)$$

where

$$l_0 = 1.08509$$

$$l_1 = 6.89715$$

$$l_2 = 13.53525$$

$$l_3 = 15.17619$$

### Numerical Approximation for $\alpha$

$$\alpha_u = \alpha \cdot \exp \left( \frac{[ p_0 + p_1/n + p_2/n^2 + p_3/n^3 + p_4/n^4 ]}{\beta} \right) \quad (4.13)$$

where

$$p_0 = 0.11254$$

$$\begin{aligned}
 p_1 &= 7.03279 \\
 p_2 &= -34.29964 \\
 p_3 &= 135.38431 \\
 p_4 &= -90.73569
 \end{aligned}$$

and

$$\alpha_1 = \alpha \cdot \exp - \left( \frac{[ q_0 + q_1/n + q_2/n^2 + q_3/n^3 ]}{\beta} \right) \quad (4.14)$$

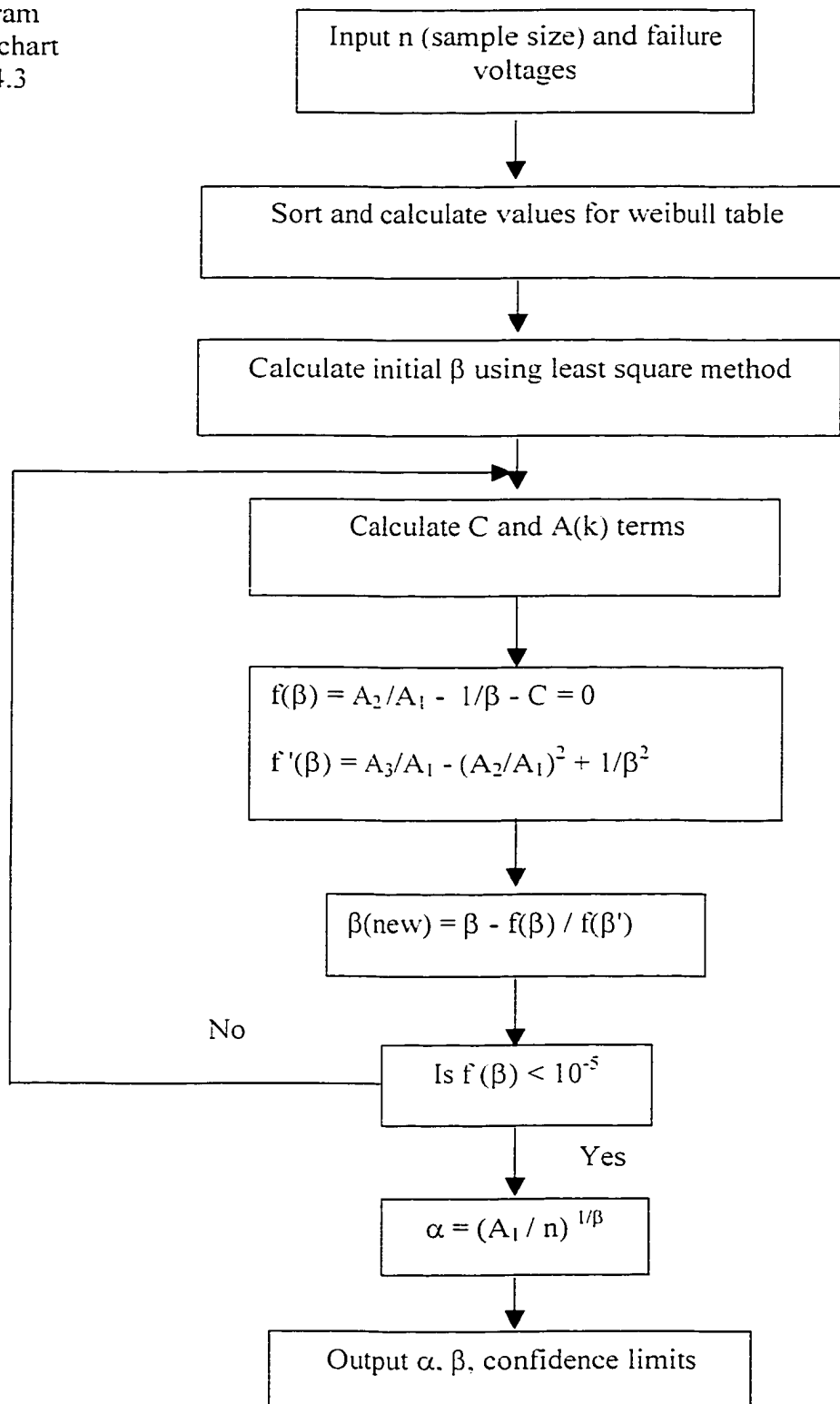
where

$$\begin{aligned}
 q_0 &= 0.10964 \\
 q_1 &= 7.33402 \\
 q_2 &= 17.70106 \\
 q_3 &= 41.43168
 \end{aligned}$$

Fig. 4.3 shows a flowchart sequence for determining  $\alpha$ ,  $\beta$  and their confidence limits. A computer program is developed in C++ by the author to calculate these entities. The program is used in determining  $\alpha$  and  $\beta$  values with 90 % confidence limits for the polymer materials tested.



Computer  
Program  
Flowchart  
Fig. 4.3



**CHAPTER 5****Experimental Analysis of PTFE, Nomex-Polyester- Nomex and Kapton****5.1 Experimental Analysis and Results for PTFE with DC voltage application**

Due to its inert property and high thermal stability, PTFE finds applications in a number of situations where chemical stability and relatively stable thermal characteristics are desirable. In this section we investigate the experimental breakdown strength of PTFE at different temperatures. Discussion on the results obtained is provided in chapter 6.

DC Voltage is applied to 50 micrometer thick samples of PTFE until breakdown is induced. The PTFE specimen is in the form of a thin film roll and the tests are performed as described in section 3.2. The tests are repeated 50 times at 12 different temperature levels each, beginning at room temperature up to 240<sup>0</sup>C. Results obtained are tabulated in table 5.1. Appendix I shows some of the results of breakdown strength investigated, in bar chart format with 50 tests at different temperature levels. The breakdown strengths have been converted to kV/mm and indicate the range of values over which breakdown occurs.

Fig. 5.1.1 to 5.1.12 show the Weibull plot of the results obtained. In order to deduce better values of  $\alpha$ ,  $\beta$  and their 90% confidence limits the computer program developed is executed and the results obtained are presented in tables in 5.1.2 and 5.1.3. Fig. 5.1.13 and Fig. 5.1.14 indicate the dielectric strength variation obtained with upper and lower confidence limits at different temperatures for the samples investigated.

23 C	40 C	60 C	80 C	100 C	120 C	140 C	160 C	180 C	200 C	220 C	240 C
7.78	2.77	12.98	10.03	1.26	8.73	9.43	2.3	7.98	8.26	6.77	6.64
6.27	8.18	11.06	9.54	9.84	6.77	4.03	10.35	9.3	5.44	6.24	6.23
5.81	3.32	11.5	10.15	8.83	1.76	8.62	8.34	7.94	3.43	1.8	1.26
6.15	7.82	10.5	10.84	5.05	3.56	7.92	8.77	9.39	5.53	7.41	4.53
7.13	7.32	8.63	2.3	9.73	9.73	7.99	7.1	2.99	8.74	6.55	5.95
10.54	8.03	10.56	9.17	10.78	11.14	8.8	8.48	9.1	8.04	7.46	5.43
11.16	11.36	8.58	12.08	9.21	9.62	6.89	5.75	8.8	7.48	7.49	1.73
8.99	12.34	11	11.54	9.9	10.64	3.84	8.51	8.41	9.38	4.49	6.76
11.32	3.72	9.22	9.02	9.14	10.16	8.34	9.44	9.07	5.55	6.61	6.78
6.7	8.32	11.29	1.86	7.89	8.6	10.83	9.1	9.12	7.91	7.8	5.87
11.67	9.41	1.46	6.8	7.96	9.48	11.29	9.08	7.42	7.43	6.59	6.36
10.24	10.12	6.43	5.5	9.27	6.58	8.44	10.44	6.22	9.23	7.45	6.41
9.96	13	8.86	10.51	11.86	9.69	11.05	11	8.43	8.61	7.77	6.09
9.75	10.89	8.36	9.5	11.93	7.34	7.37	10.33	8.98	8.88	6.49	6.82
7.8	5.06	8.81	8.6	11.74	10.45	11.08	9.04	7.5	7.9	7.3	6.85
10.57	9.42	6.92	6.4	9.94	9.83	10.53	9.97	8.35	6.86	8.14	5.71
10.25	7.92	1.79	8.63	8.54	8.4	10.01	9.77	8.97	8.58	7.5	6.32
10.13	12.73	7.66	2.66	10.6	10.16	8.78	8.43	7.8	7.29	7.58	6.27
7.53	6.53	10.74	11.59	11.23	10.23	10.46	9.38	5.5	8.99	5.88	6.06
7.52	11.06	10.22	11.55	1.12	7.83	9.76	7.2	8.25	8.51	6.53	6.67
7.95	10.88	6.55	10.58	11.58	7.91	7.86	7.23	8.24	6.05	2.83	4.77
12.59	12.86	11.1	12.05	10.13	8.93	9.13	8.9	8.9	7.41	6.93	6.88
8.34	10.32	8.01	8.25	1.33	9.67	5.96	8.17	9.36	8.22	5.43	6.41
12.73	8.81	9.44	1.68	10.53	4.25	10.48	1.06	8.23	1.55	5.45	5.87
10.6	6.93	7.56	9.68	10.62	8.3	10.61	10.57	9.66	9.46	6.14	4.89
12.4	10.9	7.93	9.38	9.75	7.86	9.57	8.55	7.95	8.94	6.56	6.78
6.96	9.67	8.96	8.81	11.37	6.73	7.08	7.34	3.98	9.05	6.81	6.37
12.3	9.97	10.85	7.93	8.5	11.98	7.46	8.21	8.96	9.6	6.24	7.09
11.52	9.21	9.86	10.35	9	8.15	9.79	10.16	7.86	8.67	6.38	1.64
9.75	1.96	12.68	7.19	7.11	9.88	6.99	4.73	4.6	6.29	5.19	6.5
7.9	10.25	7.72	7.23	10.54	10.53	6.23	8.35	6.96	7.32	2.84	5.96
11.6	7.34	10.1	10.8	11.33	11.36	9.09	3.86	10.03	9.25	7.5	5.75
8.8	10.96	10.7	9.51	8.5	9.62	7.52	5.7	9.73	4.39	6.97	6.85
10.05	8.73	11.4	9.49	11.86	8.19	9.1	7.9	8.53	8.74	6.9	5.49
1.6	6.69	7.28	11.06	9.91	10.2	9.89	7.29	5.76	8.48	7.28	6.9
6.98	4.14	8.1	9.73	7.76	10.26	10.16	13.25	6.73	2.4	6.93	1.9
11.59	10.51	10.86	8.68	12.83	10.59	8.96	3.3	7.24	8.11	7.52	6.74
10.62	3.21	11.71	7.99	12	5.33	10.15	3.82	8.7	8.44	6.49	6.35
9.24	9.25	9.16	8.86	12.56	12.24	9.46	7.49	5.6	2.96	7.24	7.47
9.36	11.14	8.02	2.79	11.93	9.57	4.88	8.74	8.36	10	5.55	7.06
12.6	12.06	2.74	11.18	4.43	8.08	11.39	8.1	8.62	6.3	7.28	7
11.7	9.79	3.91	10.53	9.19	10.8	10.35	8.67	6.9	9.06	7.82	5.99
10.63	8.47	9.04	11.88	10.37	11.52	9.46	8.95	7.96	9.41	7.67	6.07
5.08	4.18	9.02	9.36	5.28	9.52	7.83	7.95	8.33	9.45	7.61	7.12
8.53	10.46	2.84	9.51	1.31	10.79	11.41	5.88	8.79	7.43	6.5	7.02
10.28	10.21	4.14	13.06	10.81	5.78	1.76	9.52	9.94	9.33	6.93	6.94
11.9	7.31	3.22	10.5	5.66	10.47	4.64	6.6	8.36	2.48	6.89	6.69
9.88	7.36	10.7	7.62	9.03	11.28	8.31	8.8	9.41	6.02	6.97	7.23
6.68	11.43	10.1	10.57	3.04	6.59	10.92	6.89	7.34	8.18	5.5	6.22
11.59	9.42	9.02	9.88	6.66	7.68	7.57	7.42	7.08	8.54	7.3	7.05

Table 5.1.1 Results of measurements of DC breakdown voltage in kV for 50 $\mu$ m PTFE samples

Fig. 5.1.1 Weibull Plot of DC voltage B/D of 50um PTFE at 23C

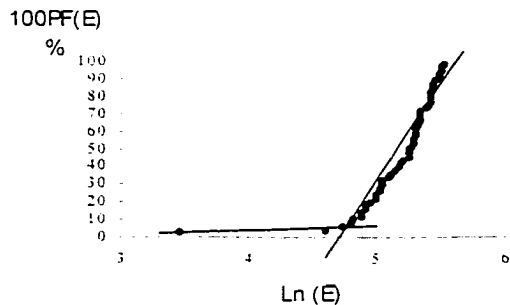


Fig. 5.1.2 Weibull Plot of DC voltage B/D of 50um PTFE at 40C

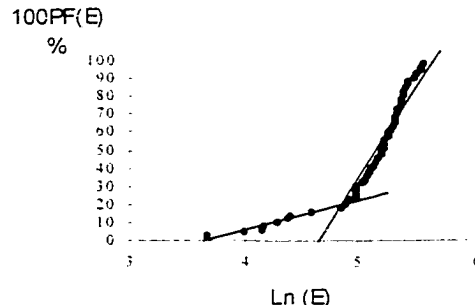


Fig. 5.1.3 Weibull Plot of DC voltage B/D of 50um PTFE at 60C

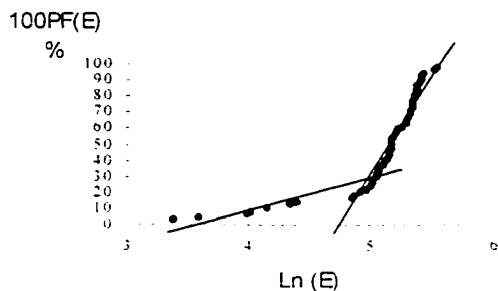


Fig. 5.1.4 Weibull Plot of DC voltage B/D of 50um PTFE at 80C

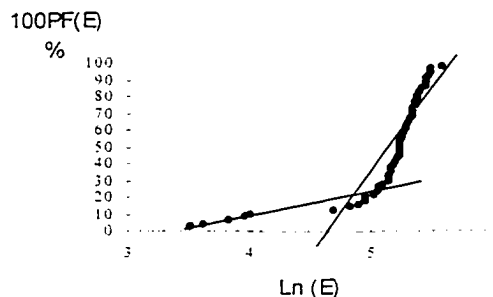


Fig. 5.1.5 Weibull Plot of DC voltage B/D of 50um PTFE at 100C

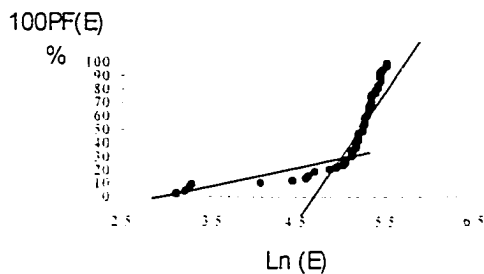


Fig. 5.1.6 Weibull Plot of DC voltage B/D of 50um PTFE at 120C

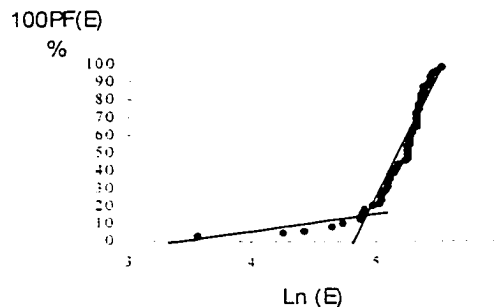


Fig. 5.1.7 Weibull Plot of DC voltage B/D of 50um PTFE at 140C

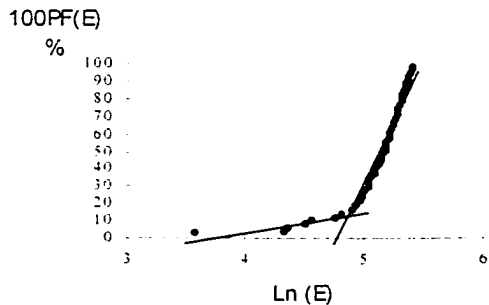


Fig. 5.1.8 Weibull Plot of DC voltage B/D of 50um PTFE at 160C

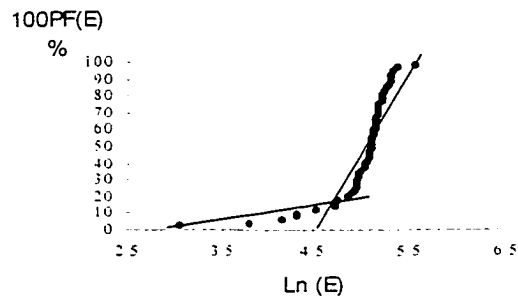


Fig. 5.1.9 Weibull Plot of DC voltage B/D of  
50um PTFE at 180C

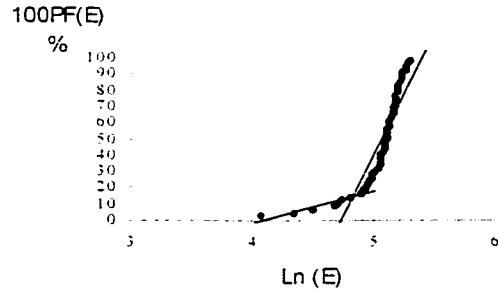


Fig. 5.1.10 Weibull Plot of DC voltage B/D  
of 50um PTFE at 200C

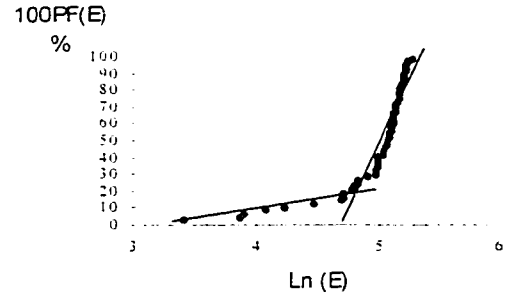


Fig. 5.1.11 Weibull Plot of DC voltage B/D of  
50um PTFE at 220C

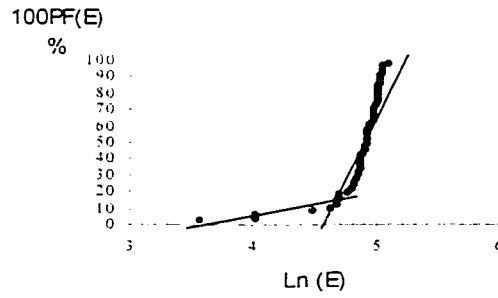
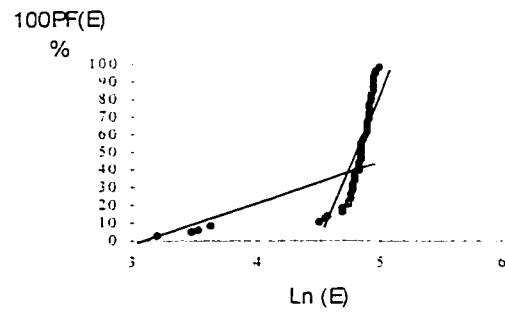


Fig. 5.1.12 Weibull Plot of DC voltage B/D  
of 50um PTFE at 240C



T(C)	betalow	beta	betaup
23	3.56	4.37	5.07
40	2.80	3.44	3.99
60	2.60	3.19	3.70
80	2.68	3.29	3.82
100	2.35	2.89	3.34
120	3.68	4.53	5.25
140	3.65	4.49	5.21
160	2.92	3.58	4.15
180	5.28	6.49	7.53
200	3.19	3.92	4.54
220	4.65	5.71	6.62
240	3.28	4.03	4.68

Table 5.1.2 Beta with 90% confidence limits for 50 $\mu$ m PTFE with DC voltage application

T(C)	alphalow (MV/m)	alpha (MV/m)	alphaup (MV/m)
23	191.4	202.6	214.2
40	177.6	190.8	204.8
60	173.2	187.2	202.0
80	178.0	192.0	206.6
100	178.4	194.4	211.4
120	182.0	191.4	202.0
140	175.4	185.4	195.6
160	160.2	171.8	183.8
180	162.8	169.2	175.6
200	151.4	161.4	171.6
220	132.4	138.4	144.2
240	119.0	126.6	134.4

Table 5.1.3 Alpha with 90% confidence limits for 50 $\mu$ m PTFE with DC voltage application

Fig. 5.1.13 Alpha with 90% confidence limits for 50µm PTFE (DC voltages)

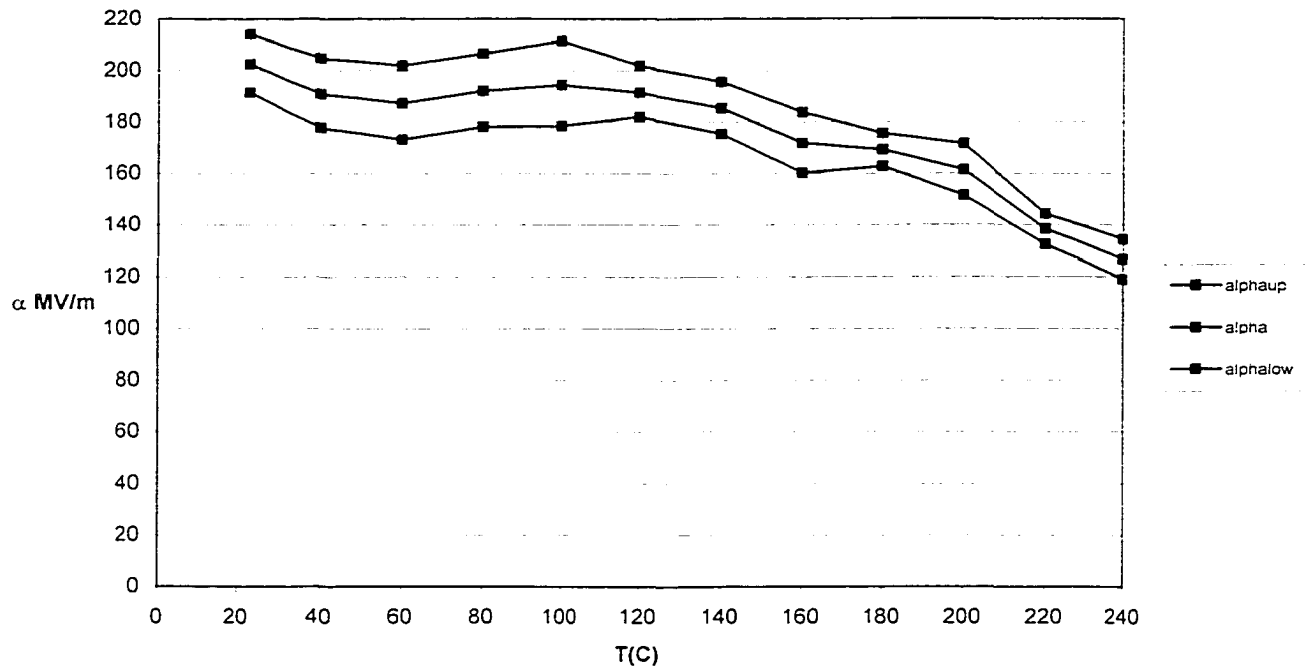
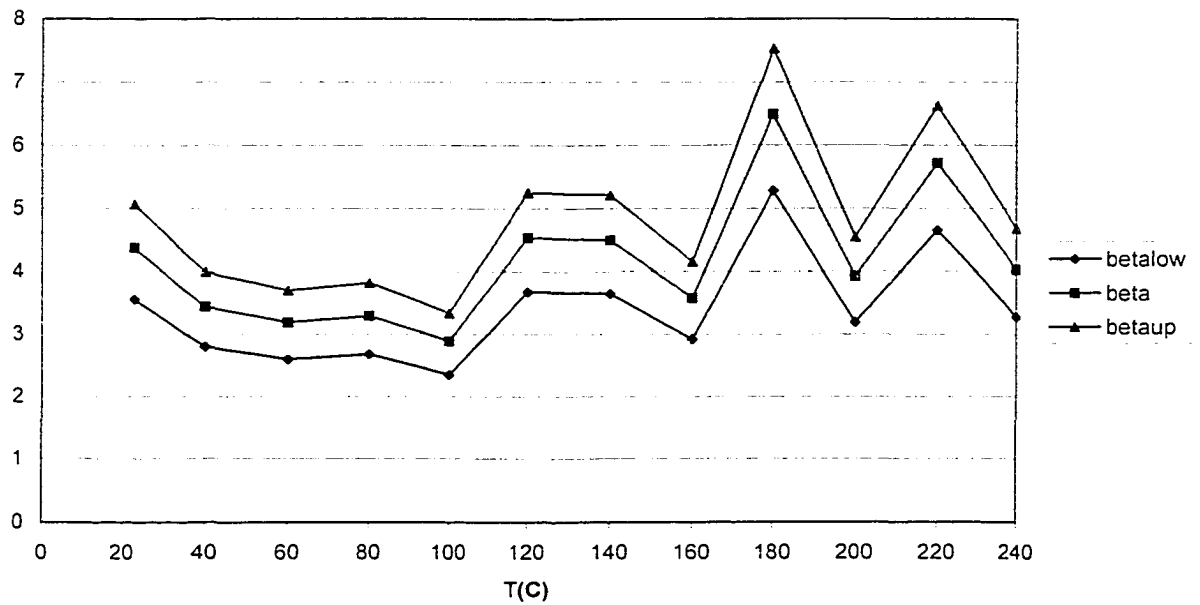


Fig. 5.1.14 Beta with 90% confidence limits for 50µm PTFE (DC voltages)



## 5.2 Experimental Analysis and Results for Nomex-Polyester-Nomex with DC voltage application

Nomex laminated with polyester fiber possesses good tensile strength and is used in environments where physical toughness is required. In this section we investigate the dielectric strength of 150 micrometer thick samples of Nomex-Polyester-Nomex with temperature. DC voltage is applied to the samples until breakdown is induced. The specimen is in the form of a thin film roll and the tests are performed as described in section 3.2.

The tests are repeated 50 times at 7 different temperature levels each, beginning at room temperature up to 140°C. Results obtained are tabulated in table 5.2.1. Appendix I shows some of the results of breakdown strength investigated, in bar chart format with 50 tests at different temperature levels. The breakdown strengths have been converted to kV/mm and indicate the range of values over which breakdown occurs.

Fig. 5.2.1 to 5.2.7 show the Weibull plot of the results obtained. In order to deduce better values of  $\alpha$ ,  $\beta$  and their 90% confidence limits the computer program developed is executed and the results obtained are presented in tables in 5.2.2 and 5.2.3. Fig. 5.2.8 and Fig. 5.2.9 indicate the dielectric strength variation obtained with upper and lower confidence limits at different temperatures for the samples investigated.

Conduction currents are measured at 140°C by applying high voltages for 30 minutes at different levels. The results are presented in Table 5.2.4. Fig. 5.2.10 shows the variation of current with time at the different voltage levels.



23 C	40 C	60 C	80 C	100 C	120 C	140 C	160 C
23.7	18.9	18.4	19.6	16.6	20.5	15.6	12.7
26.1	19.5	18.5	19.3	16.2	15.5	13.8	14.7
25.4	19.9	18.2	15.8	17.7	15.6	18.6	17.3
25.5	19.7	18.1	18.9	18.7	13.8	18.6	17.7
23.3	22.3	18.4	16.7	17.9	12.5	18.9	12.4
21.2	20.8	23.8	15.5	18.8	16	18.8	13.9
26.8	19.7	20.8	18.2	18.6	14.8	18.6	13.8
23.7	22.2	19.9	19.6	17.6	17.5	19	17.2
23.5	21.9	21.9	20.2	16.7	17.5	18.8	17.8
22.4	21.3	24.3	18.8	17.5	14.7	17.9	16
22	20.8	21.9	21	16.4	16.2	17.7	13.7
25.5	20.5	21.8	18.2	16.9	19.9	17.8	15.7
23.3	22	22.7	19.1	19.1	20.6	17.1	15.5
26.4	20.3	21	16.2	18.8	21.1	15.6	15.9
25.6	20.1	20.2	16.3	17.3	15.4	17.6	15.9
24.1	23.3	18.9	17.9	17.6	18	17.4	16.7
26.3	21.8	18.5	22.9	18.6	13.5	18.9	18.1
23.8	17.5	21.8	22.8	19.7	20.5	17.5	17.8
25.5	18.6	22.1	24.7	18.5	17.9	18.4	17.6
23.3	19.1	21.5	21	20.3	17.3	18.9	18.1
24.5	23.1	19.8	20.4	20.8	14.5	18.3	16
23.2	22.4	21.8	18.8	21.4	14.5	17.4	17
24.1	23.6	18	21.6	18.2	15.6	18.3	16.4
24.7	23.4	17.5	22.3	18.9	13.4	17.3	13.7
24.7	22.8	18.5	22.9	18	14.5	16.6	16.4
23.3	23.2	17.8	19.5	16.3	16	17.1	17.8
25.5	20.6	17.6	22.6	17.4	13.5	18.4	17.7
18.4	23.8	17	19.9	19.6	13.5	18.7	17.5
23.6	24.9	17.3	16.5	18	16.5	18.1	17.3
25.6	24.6	18.3	17.4	16.8	14.9	18.7	17.5
23.3	22.9	17.8	17.2	18.3	19.7	17.6	17.7
23.9	21.2	17.8	18	18.6	17.6	15.7	18
22.5	20.6	18.8	17.2	16.5	16.9	18.6	17.4
23.5	23.3	17.3	16.3	18.4	21.4	12.6	17.5
21.9	23.6	17.8	16.3	20.2	20.3	16.5	17.7
22.9	21	19	16	17.6	21	17.3	17.4
25.6	21.2	17.5	16.4	17.7	19	18.6	16.5
23.6	22.2	17	16.2	22.9	19.4	19.1	17.8
23.1	22.8	17.9	19.8	22	19.5	16.3	17.9
18.9	23.8	17.2	19.1	20.2	20.1	17	16.9
22.1	23.9	17.4	17.2	22.2	20.3	17	17.6
23.9	23.5	17.7	18.4	21.2	18.1	18.5	18
23.3	23.4	17.6	21.6	21.8	20.5	18.4	17.5
25.2	22.7	18.7	24.1	19.2	14.7	18.1	17.9
24.6	24	18.8	20.9	18.8	18.2	18.7	18.7
24.2	22.6	17.5	20.7	19.2	16.5	18.1	17.5
23.3	23.2	18.4	19.7	18.6	19.4	18.9	16.8
23.7	20.7	16.9	20.4	17.4	15.5	17.5	18.5
21.8	20.3	18.2	18.2	19.3	14.1	18.7	18
20.6	18.7	17.2	15.2	19.4	15.2	18.7	14

Table 5.2.1 Results of measurement of breakdown voltage for 150 $\mu$ m nomex-polyester-nomex samples

Fig. 5.2.1 Weibull Plot of DC voltage B/D  
of 150um Nomex-Polyester-Nomex at  
23C

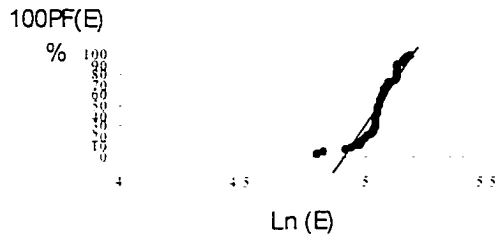


Fig. 5.2.2 Weibull Plot of DC voltage B/D  
of 150um Nomex-Polyester-Nomex at  
40C

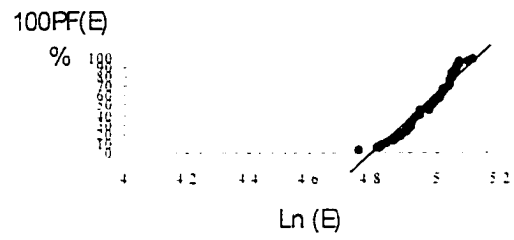


Fig. 5.2.3 Weibull Plot of DC voltage B/D  
of 150um Nomex-Polyester-Nomex at  
60C

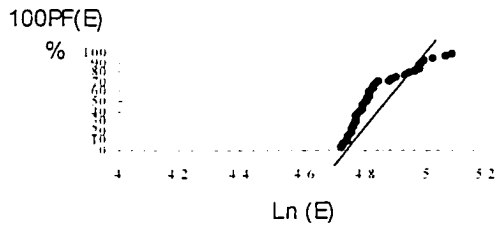


Fig. 5.2.4 Weibull Plot of DC voltage B/D  
of 150um Nomex-Polyester-Nomex at  
80C

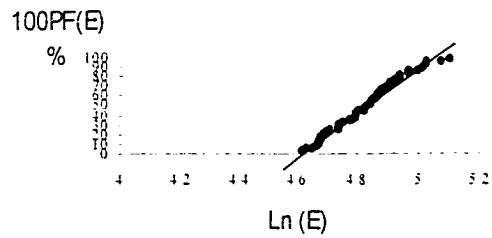


Fig. 5.2.5 Weibull Plot of DC voltage B/D  
of 150um Nomex-Polyester-Nomex at  
100C

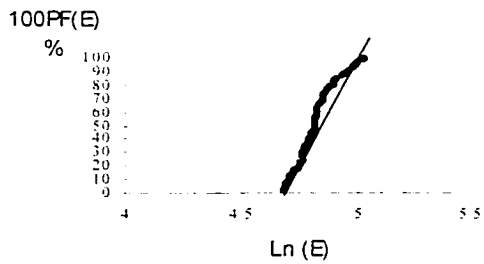


Fig. 5.2.6 Weibull Plot of DC voltage B/D of  
150um Nomex-Polyester-Nomex at 120C

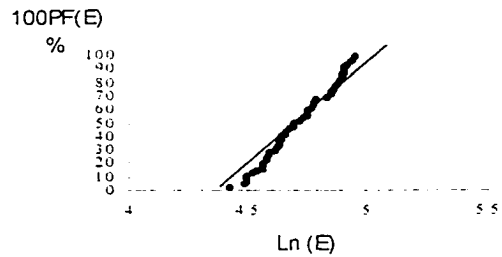
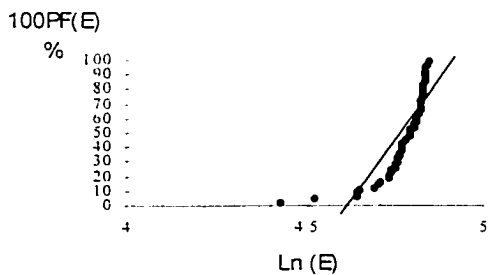


Fig. 5.2.7 Weibull Plot of DC voltage B/D  
of 150um Nomex-Polyester-Nomex at  
140C



T(C)	betalow	beta	betaup
23	13.61	16.72	19.40
40	12.07	14.83	17.21
60	7.51	9.23	10.71
80	6.77	8.31	9.64
100	8.93	10.97	12.73
120	6.15	7.55	8.76
140	15.34	18.85	21.86

Beta with 90% confidence limits for 150 $\mu$ m nomex-polyester-nomex with DC voltage application  
Table 5.2.2

T(C)	alphalow (MV/m)	alpha (MV/m)	alphaup (MV/m)
23	160.8	163.2	165.6
40	147.8	150.3	152.8
60	129.5	133.1	136.6
80	130.3	134.3	138.2
100	126.7	129.7	132.5
120	117.2	121.1	125.1
140	119.7	121.3	122.9

Alpha with 90% confidence limits for 150 $\mu$ m nomex-polyester-nomex with DC voltage application  
Table 5.2.3

Fig. 5.2.8 alpha with 90% confidence limits for nomex-polyester-nomex (DC voltages)

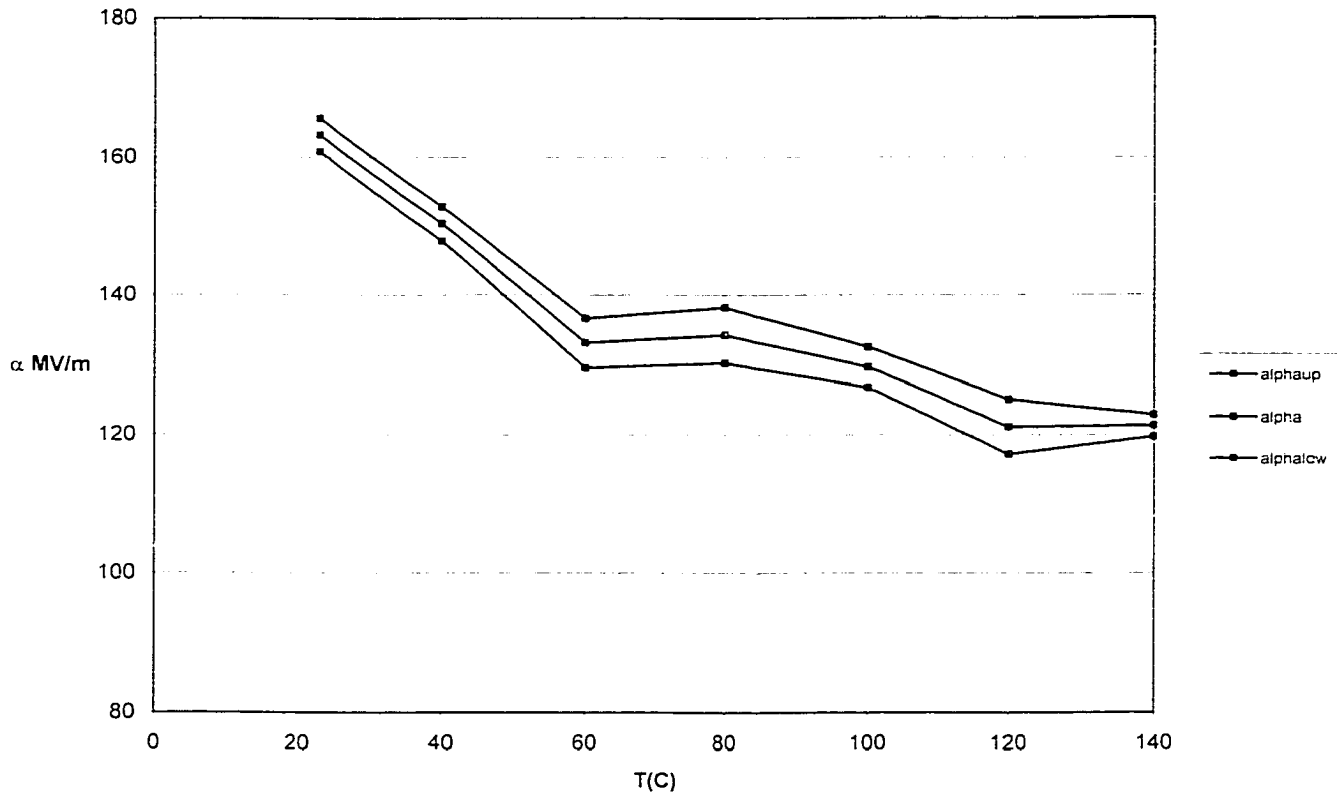


Fig. 5.2.9 beta with 90% confidence limits for nomex-polyester-nomex (DC voltages)

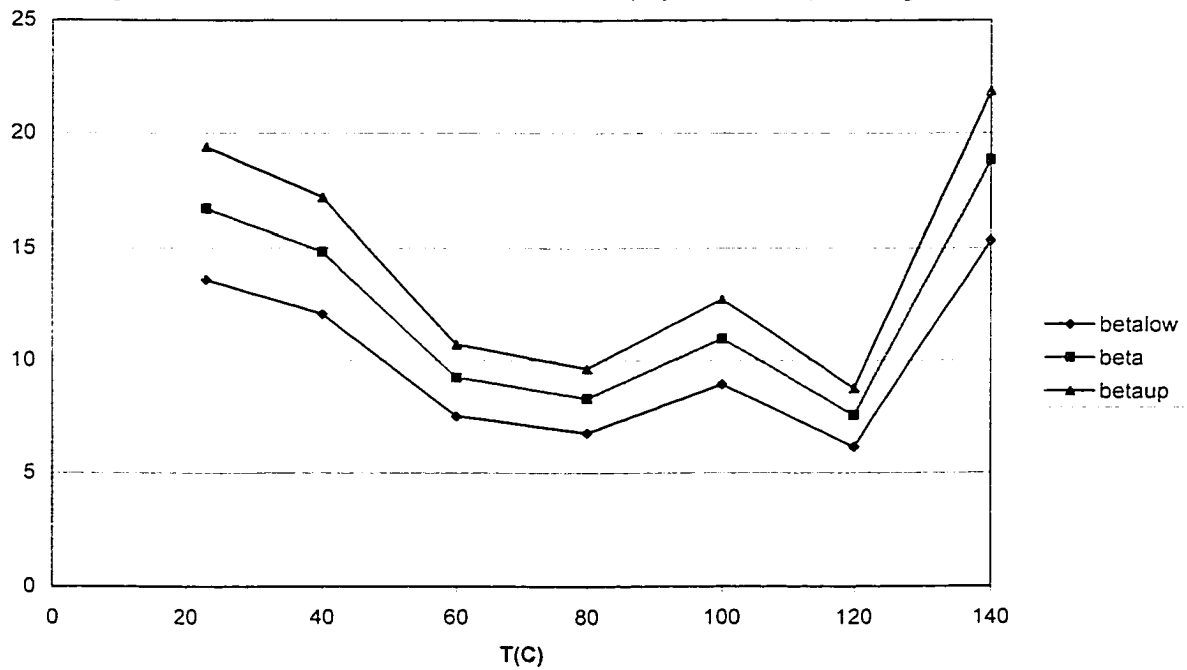
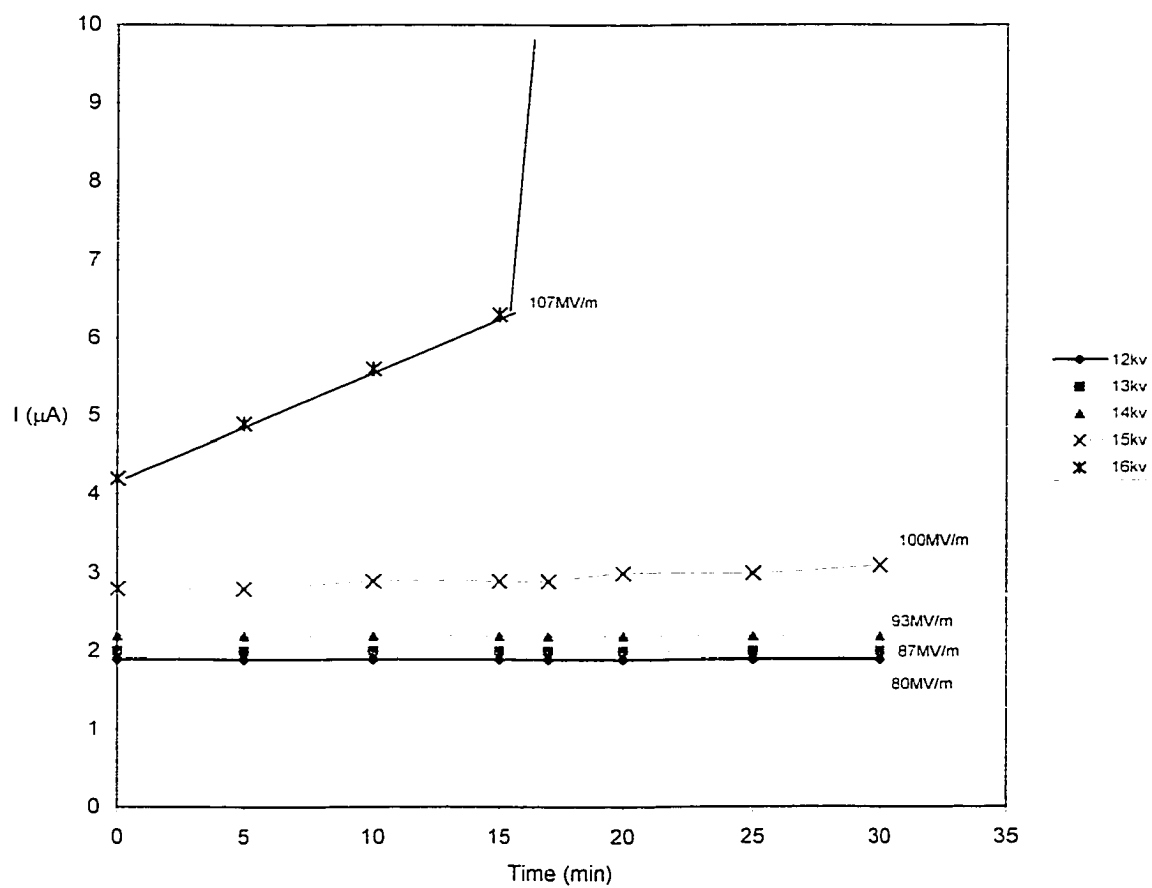


Table 5.2.4 Conduction Currents at High Electric Fields for 150 $\mu$ m Nomex-Polyester-Nomex

	80MV/m	87MV/m	93MV/m	100MV/m	107MV/m
Min / KV	12kV	13kV	14kV	15kV	16kV
0	1.9	2.0	2.2	2.8	4.2
5	1.9	2.0	2.2	2.8	4.9
10	1.9	2.0	2.2	2.9	5.6
15	1.9	2.0	2.2	2.9	6.3
17	1.9	2.0	2.2	2.9	190
20	1.9	2.0	2.2	3	
25	1.9	2.0	2.2	3	
30	1.9	2.0	2.2	3.1	

Fig. 5.2.10 Plot of current at 140C for Nomex-Polyester-Nomex at High E- Fields



### 5.3 Experimental Analysis and Results for Kapton with DC voltage application

Kapton is an organic polyimide with uses in demanding environments and applications, typically where exposure to radiation is present. In this section we investigate experimentally the dielectric strength of kapton with temperature.

DC Voltage is applied to 125 micrometer thick samples until breakdown is induced. The specimen is in the form of a thin film roll and the tests are performed as described in section 3.2. The tests are repeated 50 times at 8 different temperature levels each, beginning at room temperature up to 160°C. Results obtained are tabulated in table 5.3.1. Appendix I shows some of the results of breakdown strength investigated, in bar chart format with 50 tests at different temperature levels. The breakdown strengths have been converted to kV/mm and indicate the range of values over which breakdown occurs.

Fig. 5.3.1 to 5.3.8 show the Weibull plot of the results obtained. In order to deduce better values of  $\alpha$ ,  $\beta$  and their 90% confidence limits the computer program developed is executed and the results obtained are presented in tables in 5.3.2 and 5.3.3. Fig. 5.3.9 and Fig. 5.3.10 indicate the dielectric strength variation obtained with upper and lower confidence limits at different temperatures for the samples investigated.

Conduction currents are measured at 160°C by applying high voltages for 30 minutes at different levels. The results are presented in table 5.3.4. Fig. 5.3.11 shows the variation of current with time at the different voltage levels.

23 C	40 C	60 C	80 C	100 C	120 C	140 C	160 C
22	23.7	28.2	24.1	25.4	18	14.7	16.4
26.6	26.8	28.7	22.4	21.7	18.4	15.4	14.8
25.6	26.4	26.9	23.6	23.7	19	17.2	15.5
21.4	27.2	23.9	18.3	23.6	19.9	17.3	16.4
22.1	20.7	22.1	17.1	22.9	17.5	16.3	15.8
21.7	22.2	18.9	15.9	22.1	17	18.8	15.1
20.5	20	18.9	16.3	20.4	18.5	16.8	13.2
21.6	22.2	20.4	15.8	20.2	17.7	15.1	14.5
26.6	26.5	17.7	17	18.9	17.4	15.9	19.7
23.6	20.9	19.5	16.3	16.9	17	17.2	19.6
22.2	22.2	17.5	17.1	15.8	17.2	14.3	19.8
25.2	22.3	19.8	16.4	16.9	14.9	16.2	18.6
24.3	26.7	20.3	16.9	20	17.6	16.7	19.5
26.9	27.5	18.8	16.6	19.4	15.9	14.8	17.3
23.9	23.7	19.7	22.5	10.6	18	19	17.9
25.5	27.6	20	21	19	17.4	19.5	18.9
19	27.4	26.6	23.7	18.3	14.8	19.2	17.7
22.7	20.7	26	24.2	20.3	13.7	18.7	19.1
26.3	21.4	23.7	20.5	19.9	17.8	18.4	19.1
23.2	26.9	22.8	19.2	18.3	16.4	18	18.5
22	22.3	23.3	22.3	18.7	19.9	20.1	14.5
20.4	20.3	21.1	24.1	16	21.9	20.4	14.6
21.8	18.5	26	23.8	16	20.4	18.1	15.5
22.2	16.4	21.5	21.1	14.9	18.3	19.3	15.4
24.1	26.9	22	22.9	15.6	15.4	19.7	13.4
25.3	24.6	19.8	21.1	14	14.4	20.3	17.6
21.1	21.5	17.5	21.2	14.8	15.5	21.7	14
20.3	28.7	20.9	22.4	15.4	15.6	22.4	14.3
20	28.2	18.1	23.6	18.2	18	19.3	16.9
26.1	20.3	20.9	23.5	18.6	17.3	19.8	19.8
20.7	20.6	22	23.5	16.8	15.7	16.7	15.7
19	21.2	17.2	22	15.6	21	20.9	21.7
23.1	21.1	19.1	21.5	18.6	18.2	20.2	21.7
27.3	21.7	20.4	19.3	17.3	18.7	19.3	21.4
22.7	20.4	21.2	16.6	19.6	18.2	20.2	22.2
19.8	26.3	21.9	18.8	23.4	19.3	19.2	21
22.8	22.8	21.1	19.9	21.2	17.9	19.4	22
21.3	20.5	19.2	22.1	17.9	16.5	19.5	20.8
23.7	20.3	19	18.4	20.2	18.8	16.4	19.6
20	22.1	20.4	21.9	17.1	20.3	16.8	21.6
22	20.8	20.5	18	18.3	20.6	14.6	19.8
21.9	24.1	22	20.7	17.9	19.1	16	16.4
20.7	26	22.7	22.9	19.2	14.7	14.1	16.8
19.6	26.3	22.3	22.5	19.3	14.7	14	15.5
20.5	26.4	28.4	19	18.9	18.3	14.6	14
22.9	27.3	26.5	20.3	18.6	17	13.5	12.9
28.7	27.6	28.1	20.8	20.6	14.3	15.6	14.9
27.3	28.7	26.4	23.5	18.9	16.5	15.6	12.6
19.9	28	25.5	26.4	20.2	16.2	15.2	15.3
18.7	28.7	24.6	25.9	19.2	16.1	15.4	16.2

Table 5.3.1 Results of measurement of DC breakdown voltage for 125  $\mu\text{m}$  kapton samples

Fig. 5.3.1 Weibull Plot of DC voltage B/D of 125um Kapton at 23C

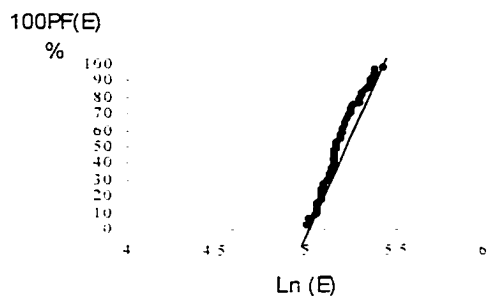


Fig. 5.3.2 Weibull Plot of DC voltage B/D of 125um Kapton at 40C

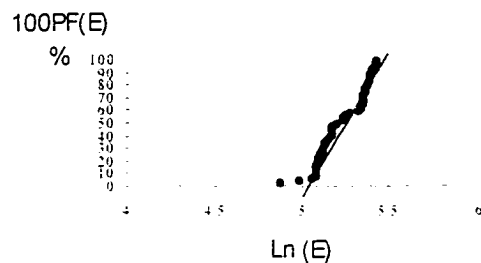


Fig. 5.3.3 Weibull Plot of DC voltage B/D of 125um Kapton at 60C

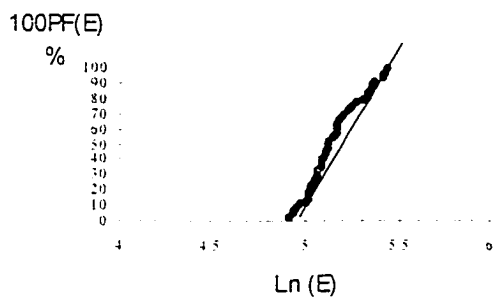


Fig. 5.3.4 Weibull Plot of DC voltage B/D of 125um Kapton at 80C

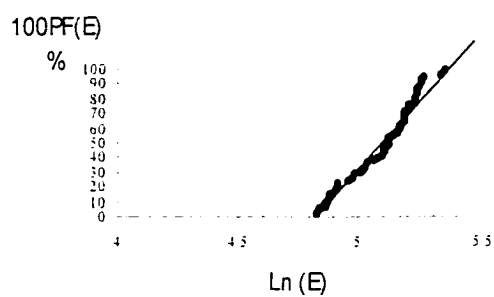


Fig. 5.3.5 Weibull Plot of DC voltage B/D of 125um Kapton at 100C

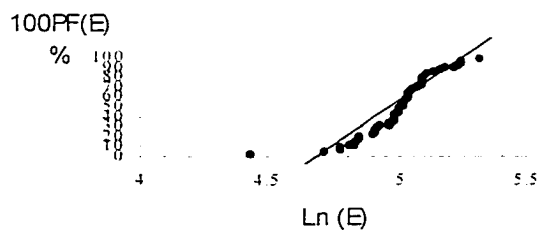


Fig. 5.3.6 Weibull Plot of DC voltage B/D of 125um Kapton at 120C

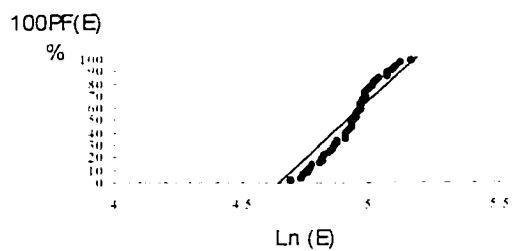


Fig. 5.3.7 Weibull Plot of DC voltage B/D of 125um Kapton at 140C

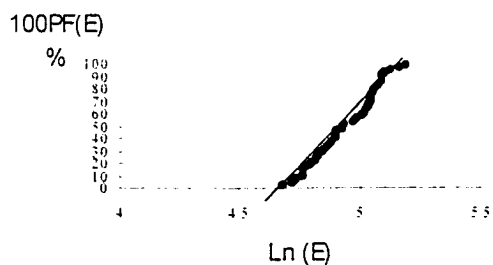
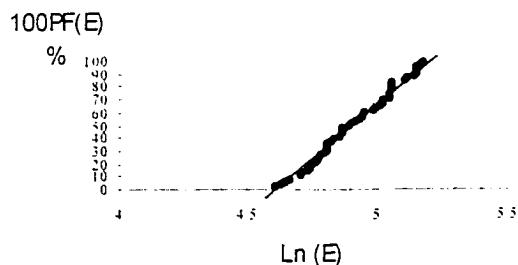


Fig. 5.3.8 Weibull Plot of DC voltage B/D of 125um Kapton at 160C





T(C)	betalow (MV/m)	beta (MV/m)	betaup (MV/m)
23	7.51	9.23	10.71
40	6.99	8.58	9.96
60	5.76	7.08	8.21
80	6.85	8.42	9.77
100	6.05	7.43	8.62
120	8.09	9.94	11.53
140	7.05	8.66	10.05
160	5.73	7.04	8.17

Table 5.3.2 Beta with 90% confidence limits for 125 $\mu$ m Kapton with DC voltage applicatio

T(C)	alphalow (MV/m)	alpha (MV/m)	alphaup (MV/m)
23	186.00	191.12	196.16
40	196.08	201.92	207.60
60	180.80	187.28	193.76
80	170.32	175.44	180.48
100	153.68	158.96	164.16
120	142.80	146.40	150.00
140	144.24	148.48	152.64
160	142.80	147.92	153.04

Table 5.3.3 Alpha with 90% confidence limits for 125 $\mu$ m Kapton with DC voltage applicati

Fig. 5.3.9 Alpha with 90% confidence limits for 125 $\mu$ m kapton (DC voltages)

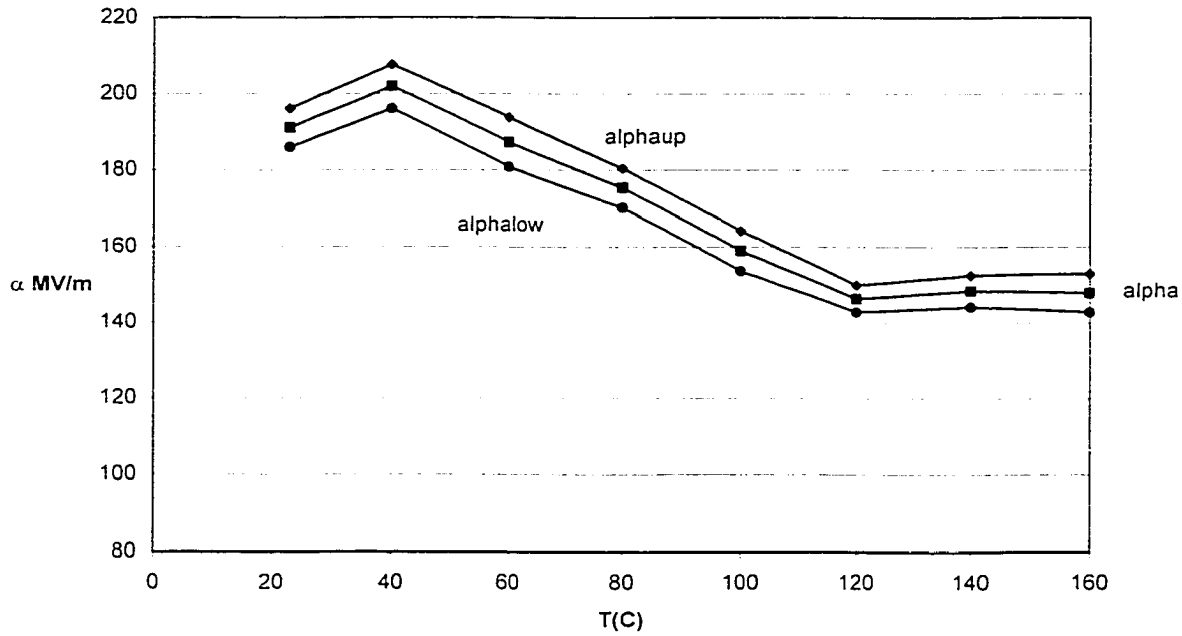


Fig. 5.3.10 Beta with 90% confidence limits for 125 $\mu$ m kapton (DC voltages)

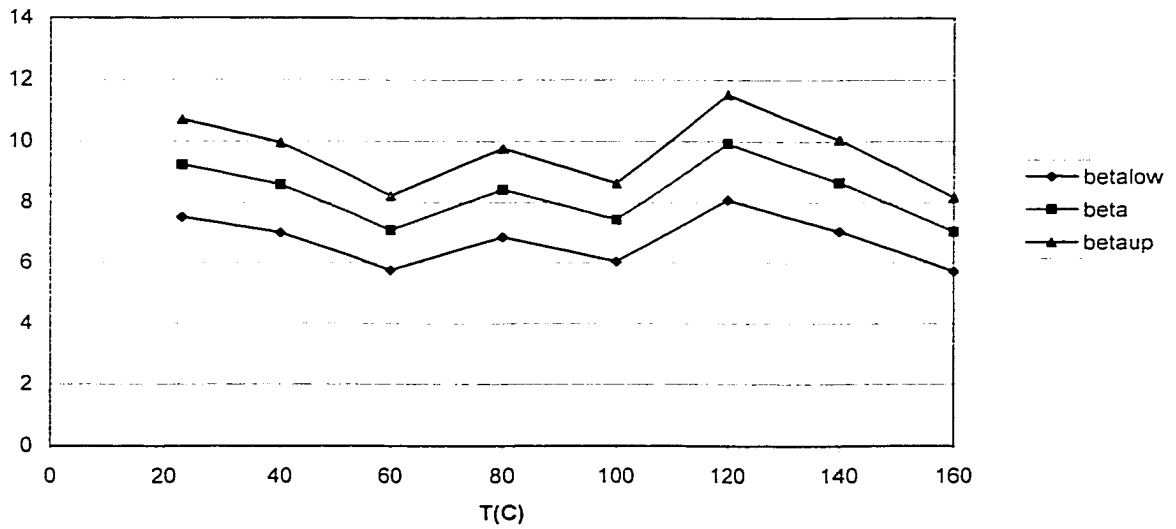
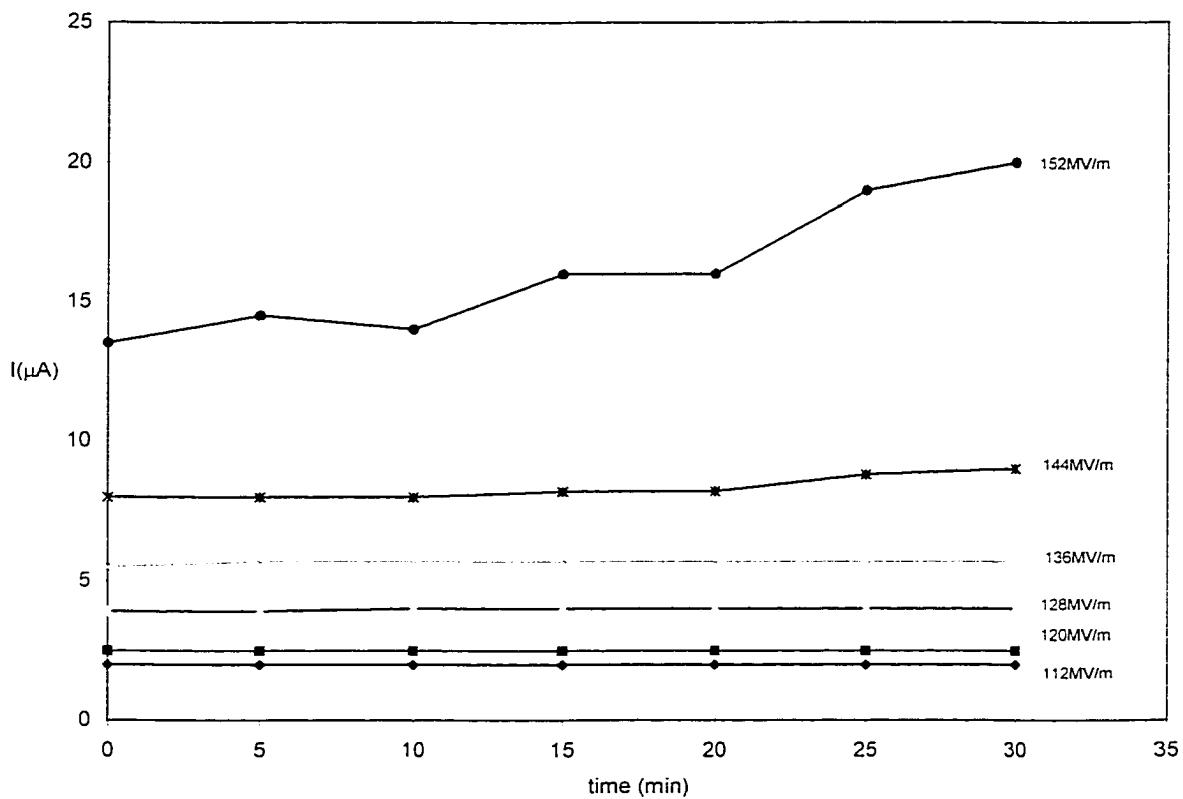


Table 5.3.4 Conduction currents at high electric fields for 125 $\mu$ m Kapton

	112MV/m	120MV/m	128MV/m	136MV/m	144MV/m	152MV/m
min / kV	14kV	15kV	16kV	17kV	18kV	19kV
0	2	2.5	3.9	5.5	8	13.5
5	2	2.5	3.9	5.7	8	14.5
10	2	2.5	4	5.7	8	14
15	2	2.5	4	5.7	8.2	16
20	2	2.5	4	5.7	8.2	16
25	2	2.5	4	5.7	8.8	19
30	2	2.5	4	5.7	9	20

Current I is in micro Amps.

Fig. 5.3.11 Plot of Current at 160C for 125 $\mu$ m Kapton at High Electric Fields

#### **5.4 Experimental Analysis and Results for Polytetrafluoroethylene with AC voltage application**

AC Voltage is applied to 50 micrometer thick samples of PTFE until breakdown is induced. The PTFE specimen is in the form of a thin film roll and the tests are performed as described in section 3.3. The tests are repeated 50 times at 12 different temperature levels each, beginning at room temperature up to 240<sup>0</sup>C. Results obtained are tabulated in table 5.4.1. Appendix I shows some of the results of breakdown strength investigated, in bar chart format with 50 tests at different temperature levels. The breakdown strengths have been converted to kV/mm and indicate the range of values over which breakdown occurs.

Fig. 5.4.1 to 5.4.12 show the Weibull plot of the results obtained. In order to deduce better values of  $\alpha$ ,  $\beta$  and their 90% confidence limits the computer program developed is executed and the results obtained are presented in tables in 5.4.2 and 5.4.3. Fig. 5.4.13 and Fig. 5.4.14 indicate the dielectric strength variation obtained with upper and lower confidence limits at different temperatures for the samples investigated.

23 C	40 C	60 C	80 C	100 C	120 C	140 C	160 C	180 C	200 C	220 C	240 C
46	45	45	47	50	48	30	42	44	44	28	40
49	50	21	25	44	44	53	46	15	21	37	37
50	55	26	50	49	13	45	41	45	45	42	38
56	46	44	52	52	43	48	43	42	40	44	12
50	59	51	45	12	42	44	44	48	43	40	27
55	50	30	30	16	29	38	37	41	40	40	40
48	48	51	35	43	52	40	47	40	47	47	40
62	50	45	35	55	49	44	46	45	44	38	42
55	39	55	45	34	53	45	40	46	30	38	46
58	54	48	50	45	50	45	45	32	26	39	45
60	50	44	44	15	47	44	48	40	43	43	39
53	54	46	54	43	52	47	47	38	39	47	45
55	55	47	22	51	53	14	20	41	40	41	45
54	44	56	56	49	45	48	45	48	47	32	36
57	47	51	49	40	51	39	48	46	43	40	44
54	50	48	46	43	40	51	50	46	44	42	42
60	50	52	49	47	42	31	47	43	45	38	42
48	44	37	49	47	42	53	39	40	46	42	40
45	38	52	53	44	44	48	41	41	44	42	42
50	10	51	49	53	51	44	45	45	48	43	37
53	50	53	48	41	48	47	50	47	43	45	42
55	50	50	51	26	45	52	32	44	47	42	41
50	41	34	53	48	20	45	40	47	38	43	42
55	12	50	55	47	48	50	15	46	37	43	43
52	48	14	51	10	47	44	40	44	44	30	40
54	45	47	55	45	44	49	46	42	40	25	39
52	53	42	44	48	47	45	44	42	45	44	40
46	41	50	52	46	48	37	35	35	44	40	37
54	50	52	40	49	40	49	45	40	37	35	15
45	49	22	54	53	23	50	49	41	42	15	38
50	52	50	15	49	50	12	47	36	40	13	37
47	47	40	50	43	45	43	43	40	21	33	41
41	45	56	49	42	41	40	45	42	33	43	41
45	55	52	51	54	39	47	48	39	37	35	42
50	39	52	50	40	27	36	49	43	44	40	36
40	49	49	54	27	52	46	13	42	48	39	34
50	52	47	41	51	47	42	47	40	43	40	42
49	50	58	54	47	48	45	48	35	30	43	43
51	49	46	45	33	39	48	40	43	13	45	35
46	52	46	53	42	50	44	43	42	45	43	42
55	54	58	48	15	49	50	50	46	34	39	42
50	46	60	54	44	39	45	38	41	43	35	36
52	53	49	45	41	46	45	44	46	43	37	36
54	42	57	28	48	40	49	48	40	46	43	42
46	33	52	34	43	49	44	42	43	47	34	40
50	54	53	47	48	46	43	47	50	48	36	37
10	24	50	48	44	51	46	41	47	47	38	42
45	48	45	52	44	45	45	40	40	46	37	42
50	50	48	52	25	47	38	41	38	45	47	41
44	48	50	47	45	50	33	31	37	45	45	39

Table 5.4.1 Results of measurements of AC breakdown voltage for 50  $\mu\text{m}$  PTFE samples

Fig. 5.4.1 Weibull Plot of AC voltage B/D of 50um PTFE at 23C

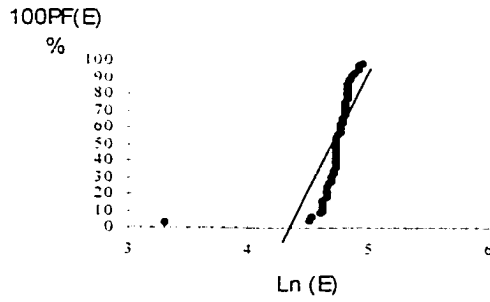


Fig. 5.4.2 Weibull Plot of AC voltage B/D of 50um PTFE at 40C

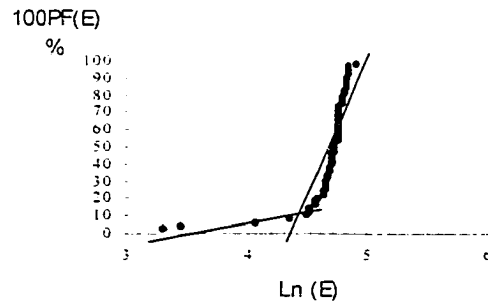


Fig. 5.4.3 Weibull Plot of AC voltage B/D of 50um PTFE at 60C

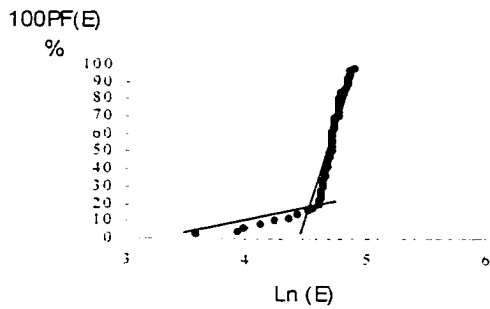


Fig. 5.4.4 Weibull Plot of AC voltage B/D of 50um PTFE at 80C

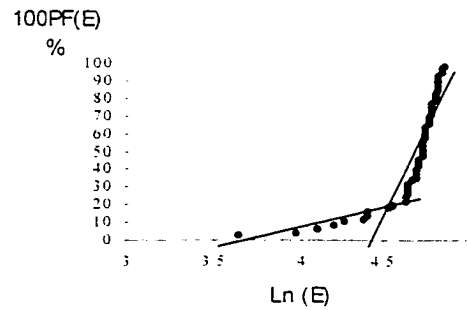


Fig. 5.4.5 Weibull Plot of AC voltage B/D of 50um PTFE at 100C

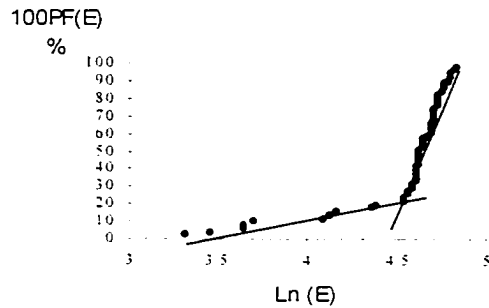


Fig. 5.4.6 Weibull Plot of AC voltage B/D of 50um PTFE at 120C

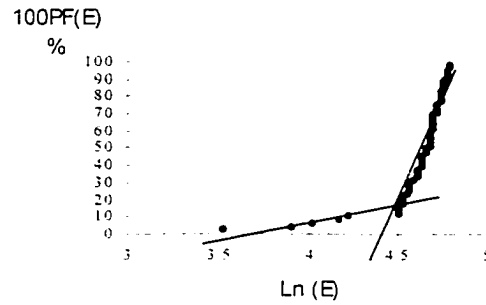


Fig. 5.4.7 Weibull Plot of AC voltage B/D of 50um PTFE at 140C

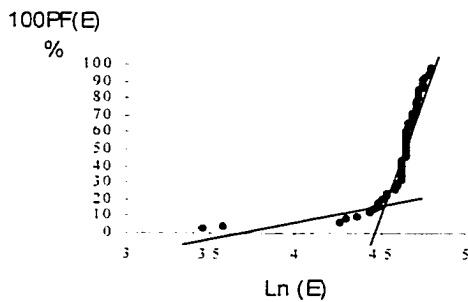


Fig. 5.4.8 Weibull Plot of AC voltage B/D of 50um PTFE at 160C

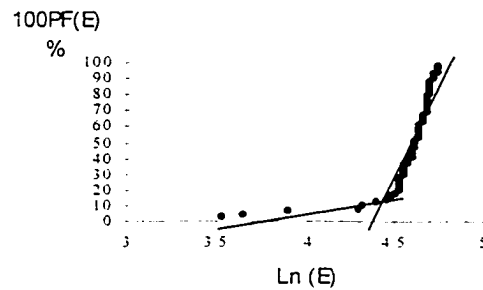


Fig. 5.4.9 Weibull Plot of AC voltage B/D of 50um PTFE at 180C

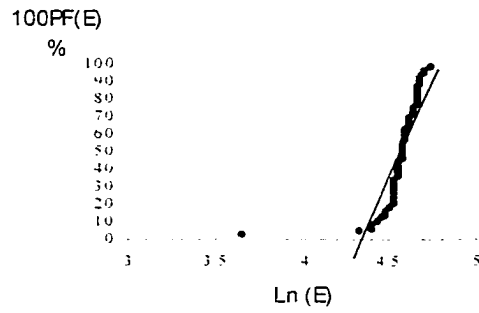


Fig. 5.4.10 Weibull Plot of AC voltage B/D of 50um PTFE at 200C

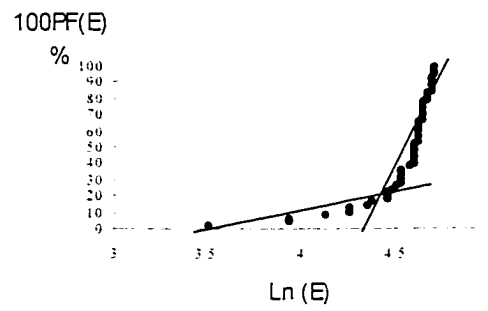


Fig. 5.4.11 Weibull Plot of AC voltage B/D of 50um PTFE at 220C

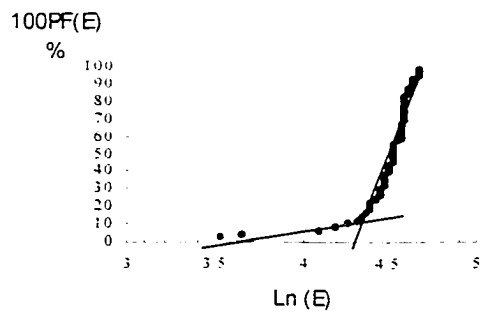
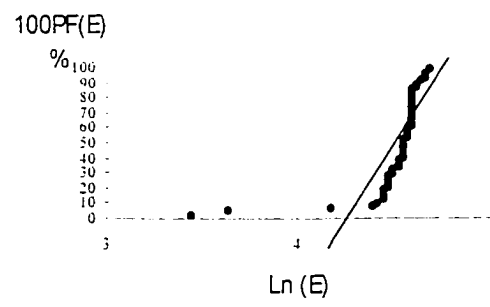


Fig. 5.4.12 Weibull Plot of AC voltage B/D of 50um PTFE at 240C



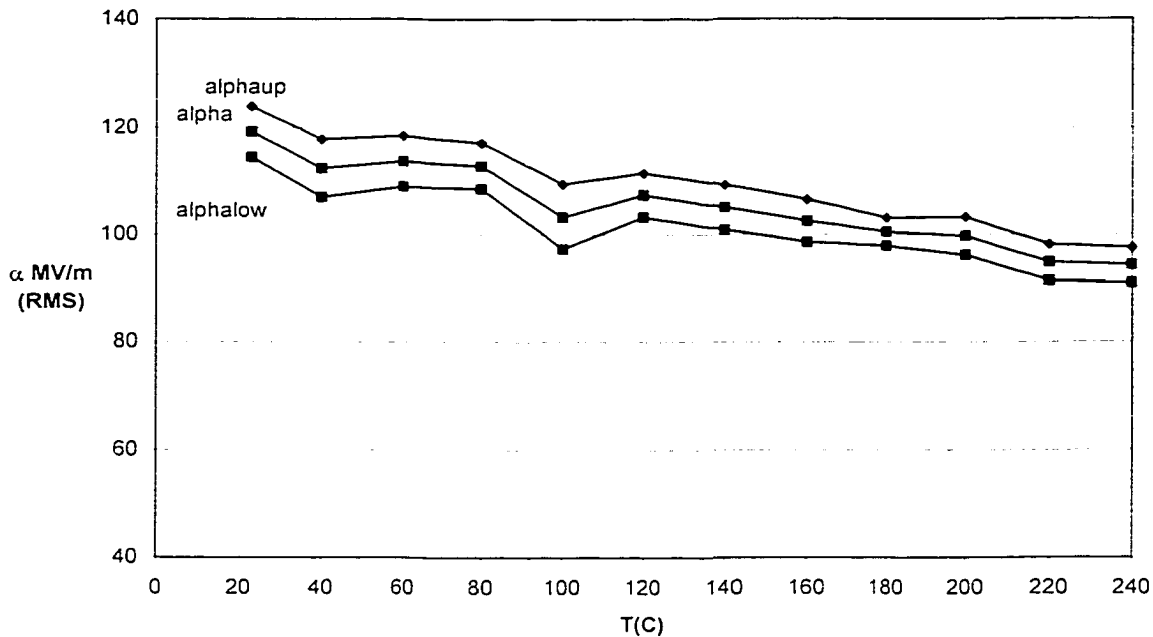
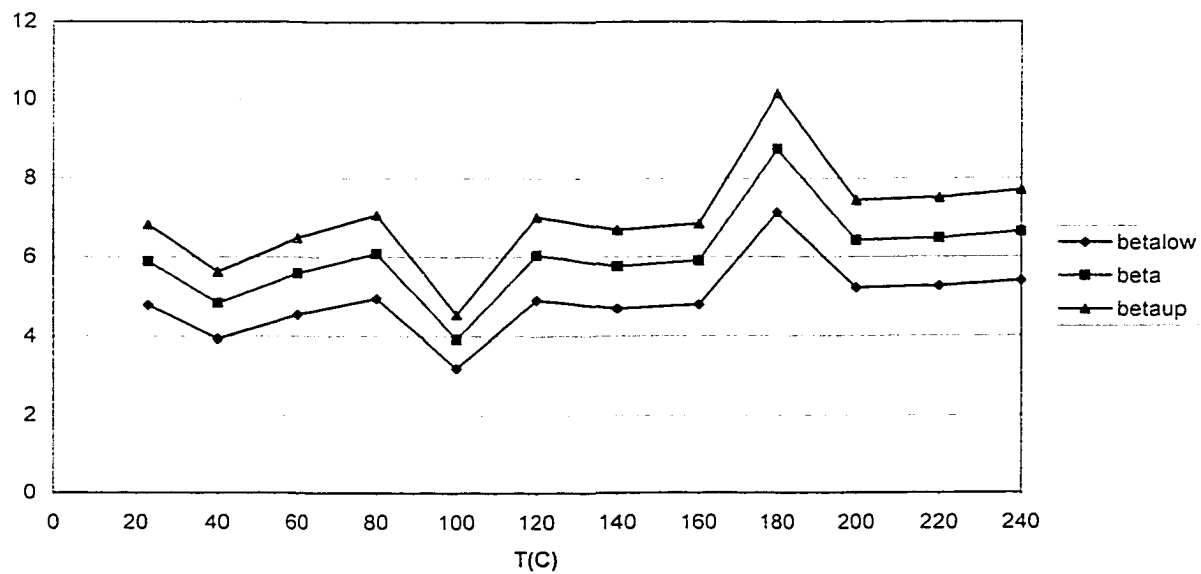
T(C)	betalow	beta	betaup
23	4.79	5.88	6.83
40	3.94	4.84	5.62
60	4.55	5.59	6.48
80	4.96	6.09	7.07
100	3.20	3.93	4.55
120	4.92	6.05	7.02
140	4.69	5.76	6.68
160	4.80	5.90	6.84
180	7.13	8.75	10.16
200	5.22	6.42	7.44
220	5.27	6.47	7.51
240	5.40	6.64	7.70

Table 5.4.2 Beta with 90% confidence limits for 50 $\mu$ m PTFE with AC voltage application

T(C)	alphalow (MV/m)	alpha (MV/m)	alphaup (MV/m)
23	114.54	119.25	123.98
40	107.04	112.41	117.85
60	109.03	113.75	118.50
80	108.57	112.87	117.19
100	97.33	103.36	109.52
120	103.36	107.48	111.60
140	100.92	105.13	109.38
160	98.56	102.57	106.60
180	97.85	100.53	103.16
200	96.17	99.76	103.36
220	91.43	94.81	98.18
240	90.99	94.28	97.55

Table 5.4.3 Alpha with 90% confidence limits for 50 $\mu$ m PTFE with AC voltage application



Fig. 5.4.13 alpha with 90% confidence limits for 50 $\mu$ m PTFE (AC voltages)Fig. 5.4.14 beta with 90% confidence limits for 50 $\mu$ m PTFE (AC voltages)

## CHAPTER 6

### Discussion and Conclusion

#### 6.1 Breakdown induced by application of DC voltages in PTFE, Kapton and Nomex-Polyester-Nomex

It is observed that by applying a steadily increasing DC voltage, the breakdown strength of the sample insulating polymer differs with each test. Hence, it is not possible to accurately associate a value for the dielectric strength for any material tested. However, discussions in terms of probability of failure are more appropriate here and can be justified by experimental data. These results are more useful to circumstantial application of material. It should be noted that in cases where there is premature failure of a dielectric at extremely low values of applied voltage, the probability is rare and can be attributed to defect dominated breakdown [16].

The cumulative probability of failure  $P_F(E)$  shows the probability that a sample will have failed by magnitude  $E$  of the electric field, with the application of an increasing field from zero. From equation (4.1) it can be seen that the probability density function and the hazard function of the two parameter Weibull distribution are:

$$G(E) = dP_F(E) / dE = \beta \alpha^{-\beta} E^{\beta-1} \exp [ - \{E / \alpha\}^{\beta} ] \quad (6.1)$$

$$H(E) = \beta \alpha^{-\beta} E^{\beta-1} \quad (6.2)$$

The shape parameter  $\beta$  plays a critical role in the statistical determination of breakdown process (section 4.3.2). In the limit of large values of  $\beta$ , many different pre-breakdown processes are involved in producing the necessary and sufficient conditions for breakdown. For values of shape parameter between one and two, the rate of increase of the hazard function decreases with time or voltage so that while the system becomes more likely to fail, the rate appears to stabilize. However, when the shape parameter is greater than two, the hazard function increases at an ever increasing rate and the system

becomes continuously more prone to failure. This suggests that pre-breakdown events produce favorable conditions for further pre-breakdown events to occur so that the rate of pre-breakdown events increases. An example of such a scenario is in avalanche breakdown. It may also happen that the final process before breakdown may influence and change the statistics of a system towards higher shape parameters. Fig. 6.1 and 6.2 show the Weibull density function generated for the test subjects at two different temperatures, 40<sup>0</sup>C and 120<sup>0</sup>C.

Fig. 6.1 Weibull Density Function for PTFE, Nomex-Polyester-Nomex and Kapton at 40C

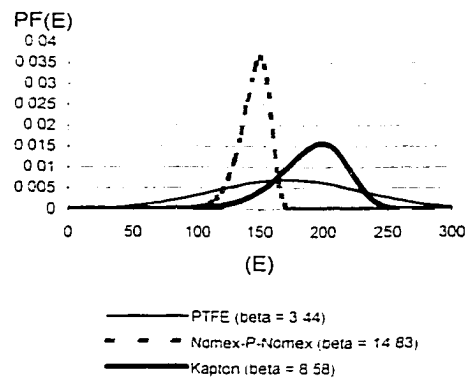
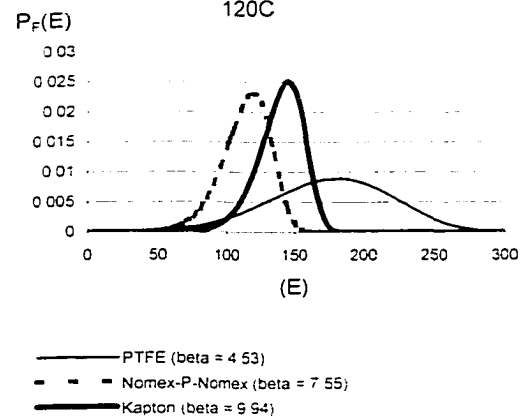


Fig. 6.2 Weibull Density Function for PTFE, Nomex-Polyester-Nomex and Kapton at 120C

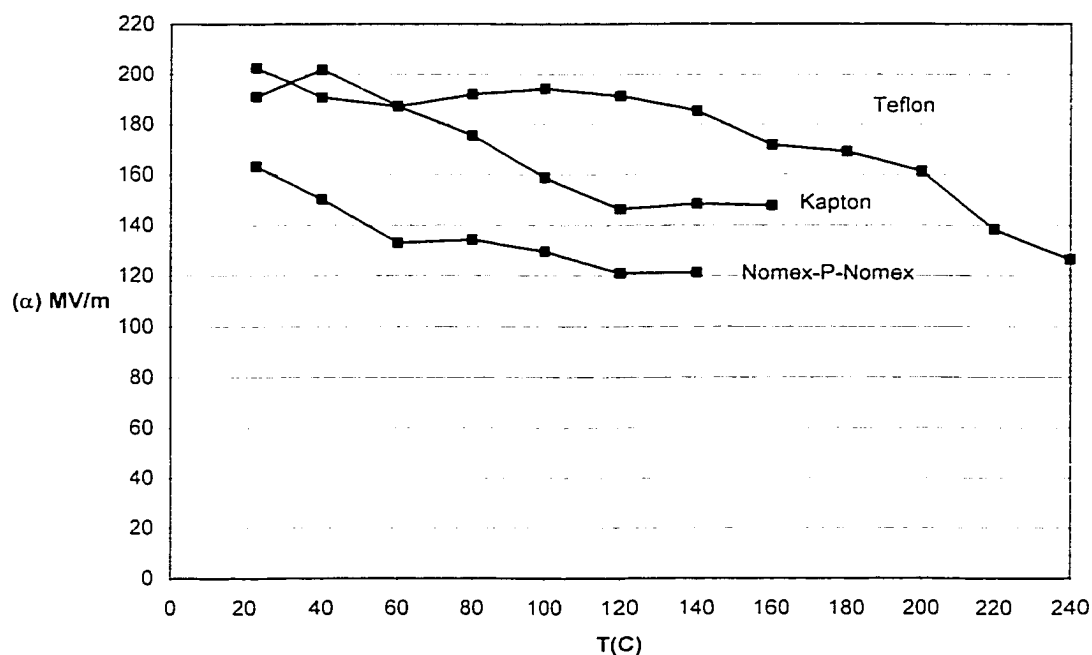


If we examine the Weibull distribution, we see that for high values of shape parameter  $\beta$ , the distribution approaches certain failure faster than those with low values. As the value of  $\beta$  is increased, the distribution becomes narrower and therefore taller, since the area under the curve is always unity, and its peak (=mode) approaches  $E = \alpha$ . It also indicates a narrower distribution of breakdown stresses in the Weibull plot, suggesting that a larger percentage of specimens will tend to fail as the applied field strength reaches a value closer to  $\alpha$ . The values of the characteristic breakdown strength is determined by the breakdown mechanism but the shape parameter contains useful information, which can help in the understanding of the fundamental mechanisms involved in the progress of breakdown.

The statistical behavior of breakdown involved here is determined by the initiation process, where breakdown can be a local process occurring in different regions of the material each differing in their local conditions, such as local field enhancement, or breakdown may involve alternative sequences of events leading to breakdown development such as discharges in voids etc.

We have also made a comparison of  $\alpha$  for PTFE, Kapton and Nomex-Polyester-Nomex tested, shown in Fig. 6.3. Alpha (excluding confidence bands) is plotted vs temperature.

Fig. 6.3 Comparison of Breakdown Strengths ( $\alpha$ ) at DC voltages



According to the temperature dependence of the dielectric strength, the temperature range can be divided into three regions. I (room temperature to 40°C), II (40°C to 160°C) and III (160°C to 240°C). While the actual characteristics of breakdown mechanism are quite complex, the general features of the types of breakdowns probable are discussed here. In the region I temperature range, it has been supported that the dominant process of breakdown under the above circumstances can be considered intrinsic [12]. This is so

since the rate of voltage application is rapid, the true characteristics of the material are exhibited ignoring defects in the physical structure. Here the breakdown field strength is considered not to depend on the size and shape of the sample, or of the material and configuration of the electrodes, but is regarded as being the characteristic of the dielectric only at some given temperature. It is also inferred that breakdown occurs in a time of microseconds or less in this type of breakdown.

In region II there are two possible mechanisms suggested which are accountable for the decrease in dielectric strength with increasing temperature: thermal breakdown and electromechanical breakdown, although some authors have also associated electronic breakdown to this region in their investigation of different polymers [13]. As can be seen from Fig. 6.3, the dielectric strength of Kapton decreases considerably with increasing temperature above 40<sup>0</sup>C. In the lower to medium temperature range of region II, thermal breakdown is attributed to the loss currents generated in the dielectric medium which promote ionic jumping and conduction at high fields. These results are also supportive of similar observations made by other authors on Kapton film [15]. The effect of thermal failure becomes more prominent at higher temperatures until 160<sup>0</sup>C where it was observed that the Kapton film had also lost its physical integrity and had reached a soft physical condition. Due to the physical state of the film and possible thinning, the local field may be enhanced giving rise to a local temperature increase and decreasing the Young's modulus. This would therefore support the theory that electromechanical breakdown is the deterministic mechanism of dielectric failure here. The dielectric strength of Kapton from our results indicate a variation from almost 200MV/m at room temperature to under 150MV/m at 160<sup>0</sup>C.

A similar condition is also observed with Nomex-Polyester-Nomex where the affect of temperature starts becoming more prominent and the dielectric strength starts reducing when the surrounding temperature was raised above room temperature. At high temperatures in the region of 140<sup>0</sup>C, the affect of partial discharges is observed. Fluctuating discharge currents were observed just before breakdown in the Nomex-Polyester-Nomex film resulting in a drop of voltage across the specimen, eventually

leading to dielectric failure. This may be attributed to the voids or defects and the compound effect of contaminants that may be present in the nomex and polyester layers of the film tested during manufacture. Also, at higher temperatures in this region, polyester tends to lose its solid state affecting the structure and the chemical nature of the compound material. It can also be related that exposure to high temperatures create thermally stimulated discharge currents which result in the weakening of dielectric strength over a period of time [14]. The dielectric strength of Nomex-Polyester-Nomex from our results indicate a variation from almost 165MV/m at room temperature to around 120MV/m at 140<sup>0</sup>C.

PTFE seems to exhibit very good characteristics of dielectric strength over the temperature range of regions I and II. It is observed to be fairly constant in these regions showing its thermal integrity over a wide range of operating temperatures. However, above 160<sup>0</sup>C, the dielectric strength of PTFE decreases significantly with increasing temperature indicating that thermally induced breakdown and electromechanical breakdown are becoming the prominent factors. Also, it is observed that during breakdown the dielectric film is punctured. No signs of partial discharges were observed prior to breakdown even at high temperatures in the PTFE film and good physical integrity of the material was observed up to 240<sup>0</sup>C. Some of the failure results obtained at lower values of applied field can be associated with microscopic defects that may be present in that region of the polymer film. The dielectric strength of PTFE from our results indicate a variation from around 200MV/m at room temperature to around 125MV/m at 240<sup>0</sup>C.

## **6.2 Breakdown induced by application of AC voltages in PTFE**

Although the bulk of experience with lifetime predictions has been obtained on AC operating systems, the deterministic breakdown theories have been developed in terms of applied DC fields. It is usually assumed that the DC breakdown field for a particular mechanism is equivalent either to the field amplitude  $E_b$  or peak to peak value  $2E_b$  of the characteristic breakdown stress in a distributed process under AC conditions.

Taking this relationship into account, the statistical analysis of accelerated and ramp DC breakdown tests have typically been made in the same way as for the AC case. This procedure however, is not always valid since alternating stress automatically introduces both physical and statistical factors that are not necessarily present in the DC case.

By definition an alternating field changes polarity twice each cycle and will thus cause any field dependent factor to range from zero to a maximum on each half cycle. The system therefore experiences, in effect, a series of pulses in those factors that cause breakdown when a critical value is exceeded. Statistically each pulse represents an attempt to fail, and the overall survival probability is the joint survival probability for the number of pulses. On the application of DC fields, the system experiences no such repetitive stress pulses. Instead it might be expected that either an equilibrium is eventually established or that the system proceeds to breakdown in a given time i.e. deterministic breakdown. However, this is an oversimplification since stochastic events may be responsible for both initiation and propagation to breakdown leading to a statistical description. In view of the difficulty in achieving a purely empirical analysis of DC breakdown statistics, it is vital that a fundamental understanding of the features specific to DC fields be obtained so that the statistical data can be interpreted with any confidence.

When an alternating field is applied to a uniform dielectric, both current density and polarization alternate in phase with the field. The time dependent polarization also generates a displacement current which is  $90^{\circ}$  out of phase with the field. Most theories relate breakdown to charge displacement in one form or another, for example via the onset of a runaway current or by the build up of local space charge concentrations sufficient to cause failure through local electrostatic forces. Alternating fields therefore place the dielectric at risk of failure once every half cycle if the direction of charge flow is immaterial and every cycle otherwise. If the injection currents are polarity dependent, space charge may build up progressively, and in addition local damage and deformation

may be accumulated thereby causing fatigue in the insulation. Therefore under alternating fields, a dielectric experiences repetitive attempts to fail as it ages.

Under the application of a DC field, the dielectric initially experiences a transient behavior as the polarization and current density relax to their static values. Only if the current density locally exceeds a critical value will the system runaway to breakdown. Otherwise an equilibrium current density will be reached. During the transient period current gradients will exist at the injecting or extracting electrodes and space charge will build up to a steady state value. Dielectric breakdown would not therefore occur at DC voltages below those required for deterministic mechanisms if it were not for the possibility of fluctuations. Structural fluctuations may cause local variations in charge density leading to local current enhancement and causing damage to the dielectric. Rapid polarity reversals may be particularly severe in this respect since here the space charge transiently increases the field near the electrodes to a considerable extent producing large injection currents which may even reverse before the system returns to equilibrium. A substantial risk of damage exists during this process.

In a system containing space charge, the local field will vary considerably from place to place in the material and be controlled substantially by space charge concentrations and their fluctuations. It may therefore be better to describe the state of the system through the distribution of local space charge concentrations that it contains. Here breakdown would occur when a critical local space charge density is exceeded. Dissado and Fothergill [11] show that for a progressive stress test, where we assume that injection continuously builds up space charge at the injecting point until sufficient is present to initiate a rapid runaway process causing near instantaneous failure, the estimated DC field strength is given by

$$E_{\text{bdc}} = [ \rho_c^\delta / A ]^{1/(\Delta - \delta - 1)} \quad (6.3)$$

where  $\rho_c$  is the charge density,  $\delta$  is the loss factor,  $\Delta$  is the rate of change of field strength to impulse breakdown and  $A$  is a proportionality constant. The above estimate is



independent of ramp rate. This result applies formally to a deterministic situation i.e. breakdown only occurs when the characteristic field is applied and then instantaneously, and can be taken to apply to the impulse limit i.e.  $\Delta \rightarrow \infty$ .

The equivalence to the DC breakdown field shown above can be obtained by substituting the equivalent power law form which determines the DC characteristic breakdown strength. In terms of the RMS value the breakdown field is

$$E_{\text{bac}} = (1/\sqrt{2}) [\rho_c^\delta / A]^{1/(\Delta-\delta-1)} \quad (6.4)$$

So in the case where there is no initial charge density, the ratio of equivalent DC field strength to RMS AC characteristic breakdown strength is  $\sqrt{2}$ . Note that in practice  $\Delta$  is less than infinity, the AC breakdown strength is less than that of the impulse limit equation (6.4) and hence the ratio may be greater than  $\sqrt{2}$ .

A comparison of the dielectric strength for DC and AC voltages is shown in Fig.6.4. The RMS AC values have been converted to peak to peak values ( $\sqrt{2}$  RMS) for comparison with DC values. The results are supportive of the above analysis in that the DC breakdown strength is greater than  $\sqrt{2}$  RMS AC strength, because of a finite rate of change of voltage during ramp up. A comparison of beta between DC and AC voltage application is also shown in Fig. 6.5 for PTFE.

Fig. 6.4 Alpha for 50um PTFE DC and AC Voltage Comparison

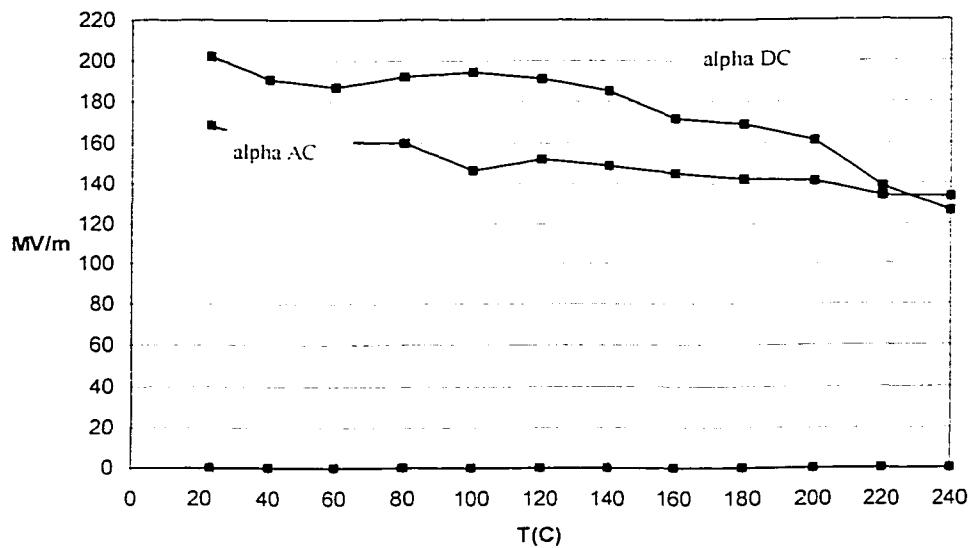
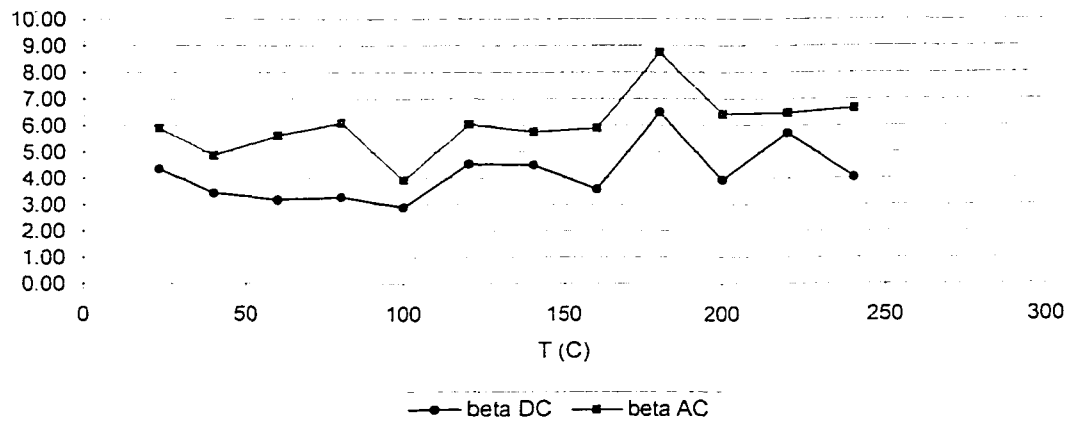


Fig. 6.5 beta for 50um PTFE DC and AC Voltage Comparison



### **6.3 Electrical conduction in Kapton and Nomex-Polyester-Nomex at high fields and temperature**

Results from Fig. 5.3.11 indicate that there is little variation in the conduction current with time when the electric field applied is in the range of 112MV/m to 144MV/m at 160°C. In this range it is observed that the relationship of steady state DC current with the electric field is ohmic. This appears to be consistent with the results of other authors who also observed a similar relationship [18]. While there is no reasonable agreement between the various workers who have carried out similar investigations, it is strongly supported that the conduction at high fields in Kapton is ionic. When the applied electric field strength is greater than 150MV/m, it is seen that the conduction current increases gradually with time. This may be explained on the basis of charging currents where there is accumulation of positive charges within the polymer close to the cathode. The ions originate within the bulk of the material or are injected from the anode and drift towards the cathode, thereby increasing the cathode field [19].

Fig. 5.2.10 also shows that there is little change in conduction current with time when the electric field applied is in the range of 80MV/m to 100MV/m at 140C for Nomex-Polyester-Nomex. However, it is seen that the current starts increasing gradually with time at higher fields indicating that effects of isothermal charging currents are in progress. The relationship of steady state DC current with the electric field in this region can also be seen to be ohmic.

### **6.4 Factors affecting accuracy of tests**

Although we have tried to minimize the variation in external conditions between successive tests based on the experimental setup, some factors which need to be considered that have influenced the accuracy of results obtained, and are beyond our means of control with this particular setup are:

- Uniformity of temperature through the chamber at any given temperature

- Effect of prolonged heating on polymer films especially at higher temperatures affecting the physical characteristics of the tested material
- Thickness variation between samples of the same film
- Contaminant material deposited on electrodes with successive tests affecting electrode-film interface
- Variation in the rate of change of applied voltage between successive tests

### **6.5 Suggestion for Future Work**

There is little published information about the dielectric breakdown strength for multiple layers of an insulating polymer compared with the same total thickness of a single layer of the same material. It is suggested that further studies be conducted on polymers for comparison of dielectric strength and breakdown mechanisms between mono-layer and multiple layer samples of the same insulating material using both AC and DC voltages.

There is also little information available on the effects of the rate of voltage rise during stress tests, which may influence several factors leading to breakdown strength. Tests should therefore be performed at different rates of increasing voltages and the breakdown characteristic obtained be compared with that of the impulse breakdown characteristic.

## APPENDIX I

Distribution of B/D strength in bar chart format

Fig. I.1 Distribution of DC B/D strength of 50um PTFE at 23C

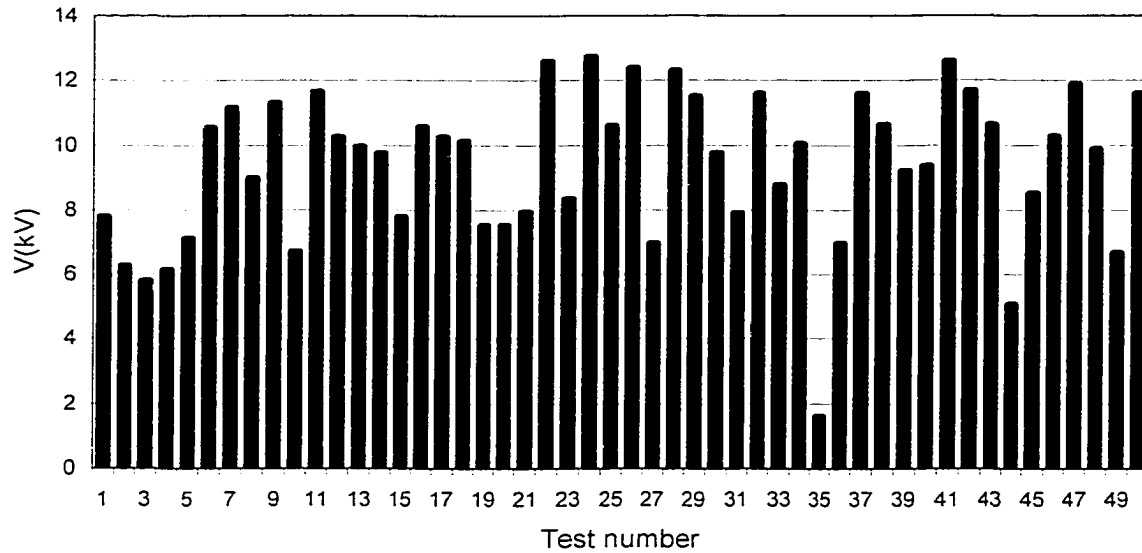


Fig. I.2 Distribution of DC B/D strength of 150um Nomex-Polyester-Nomex at 120C

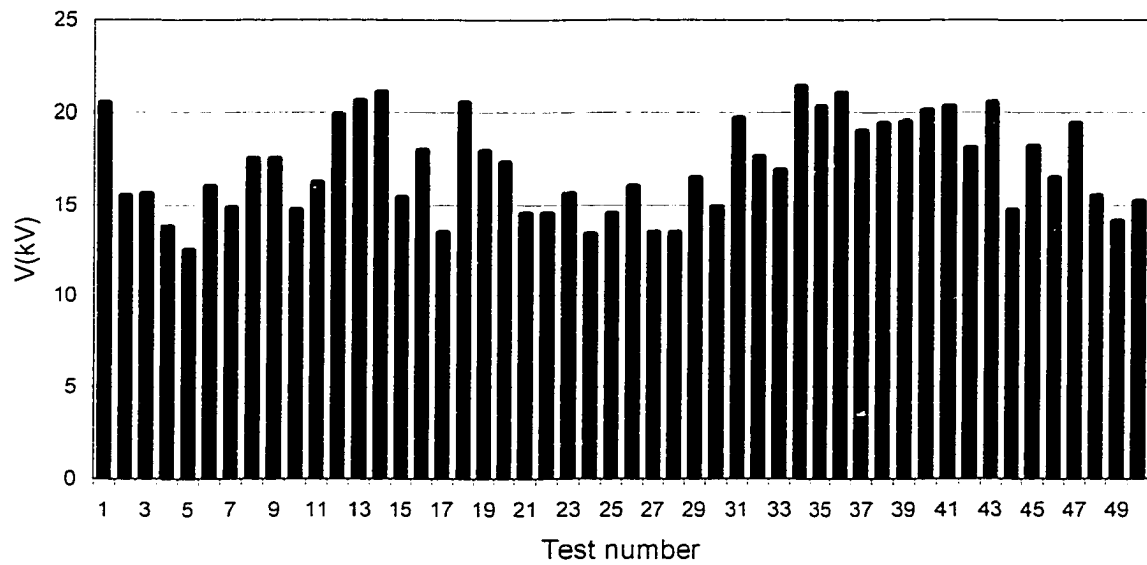


Fig. I.3 Distribution of DC B/D strength of 125um Kapton at 60C

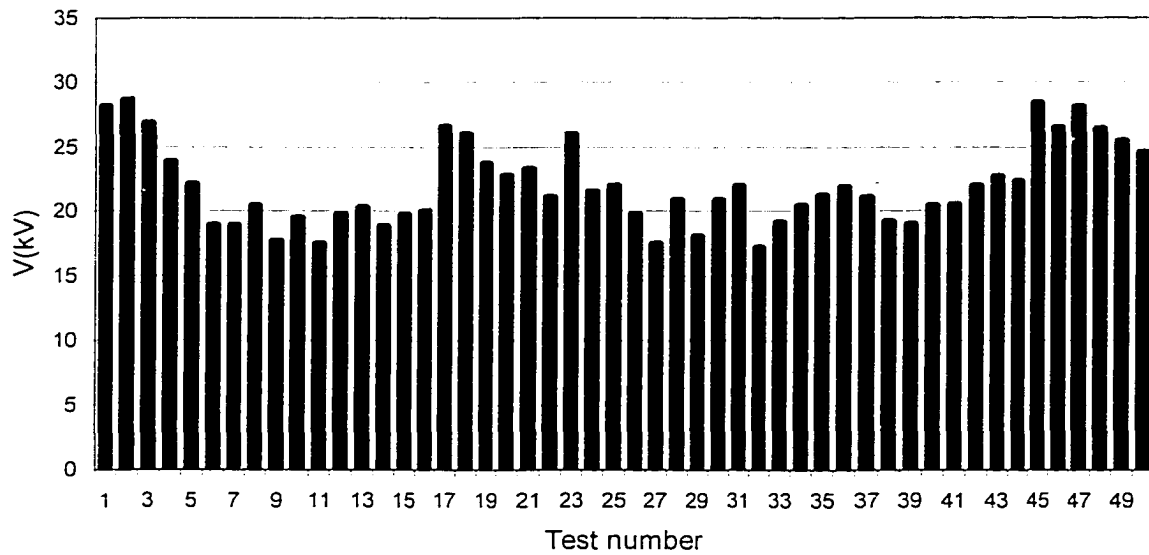
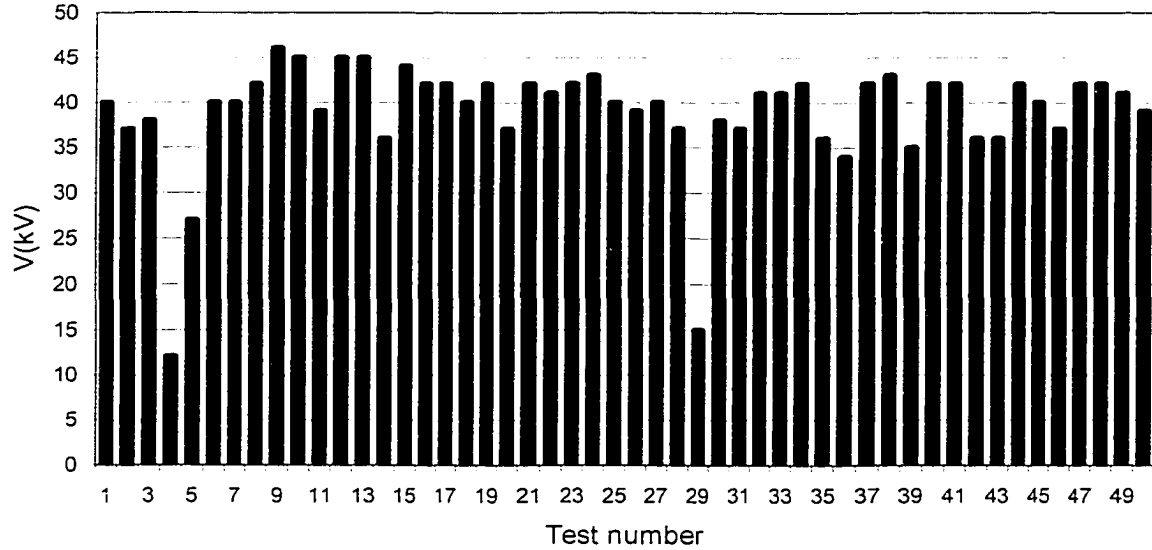


Fig. I.4 Distribution of AC B/D strength of 50um PTFE at 240C



## Appendix II

Computer Program in C++ for calculating parameters alpha, beta and their 90% confidence limits

```
#include<iostream.h>
#include<math.h>
#include<iomanip.h>

const int max_size = 60; //MAXIMUM NUMBER OF SAMPLES AT ANY ONE TIME

void selection_sort(double[], int); //FUNCTION PROTOTYPE FOR FUNCTION
THAT

//SORTS THE VOLTAGE ARRAY IN ASCENDING

//ORDER

//START OF MAIN PROGRAM
void main()
{
//VARIABLE DECLARATIONS
double voltage[max_size], R[max_size], S[max_size], x[max_size], y[max_size],
SUMxy, SUMx, SUMy, SUMx2, SSxy, SSxx, beta1, beta,
SUMn, C, A[3], f, dif, alpha,
WU, WL, betaUP, betaLOW,
Zurn, ZU, ZL, alphaUP, alphaLOW;

int size, i, k;

//-----
//PROMPT & READ INPUT
cout<<"Please enter the number of samples: ";
cin>>size;

cout<<"Please enter failure voltages:\n";
for(i=1; i<=size; i++)
{
    cout<<i<<" ";
    cin>>voltage[i];
}

//-----
selection_sort(voltage, size); //SORTING VOLTAGE ARRAY IN ASCENDING
ORDER
```

```

//FUNCTION CALL

//-----
//FOR EACH SAMPLE ENTERED (i=1 TO SIZE), CALCULATE R, S, Y & X
for(i=1; i<=size; i++)
{
    R[i] = (double(i))/(double(size+1));
    S[i] = 1.0 - R[i];
    y[i] = log(log(1.0/S[i]));
    x[i] = log(voltage[i]);
}

//FOR EACH SAMPLE ENTERED (i=1 TO SIZE), CALCULATE THE REQUIRED
SUM ARGUEMENTS
SUMxy = 0; SUMx = 0; SUMy = 0; SUMx2 = 0; //INITIALIZE SUM
ARGUEMENTS
for(i=1; i<=size; i++)
{
    SUMxy = SUMxy + (x[i]*y[i]);
    SUMx = SUMx + x[i];
    SUMy = SUMy + y[i];
    SUMx2 = SUMx2 + (x[i]*x[i]);
}

//CALCULATE SSxy & SSxx USING THE SUM ARGUEMENTS CALCULATED
ABOVE
SSxy = SUMxy - ((SUMx*SUMy)/(double(size)));
SSxx = SUMx2 - ((SUMx*SUMx)/(double(size)));

beta1 = SSxy/SSxx; //CALCULATE SLOPE OF BEST FIT LINE

//-----
//OUTPUT
cout<<setprecision(5)<<endl<<endl; //SET ALL FLOATS TO 5 DECIMAL PLACES

//HEADER
cout<<setw(10)<<"Sample#"<<setw(10)<<"Voltage"<<setw(10)<<"R(i,V)"
    <<setw(10)<<"S(i,V)"<<setw(10)<<"y"<<setw(10)<<"x"<<endl;
cout<<"-----\n";

//DISPLAY VALUES THAT WERE READ FROM INPUT & CALCULATED IN
COLUMNS (WIDTH 10)
for(i=1; i<=size; i++)
    cout<<setw(10)<<i<<setw(10)<<voltage[i]<<setw(10)<<R[i]<<setw(10)<<S[i]
        <<setw(10)<<y[i]<<setw(10)<<x[i]<<endl;

```



```

cout<<"\nINITIAL BETA = "<<beta1<<endl;

//-----
SUMn = 0;
for(i=1; i<=size; i++)
    SUMn = SUMn + log(voltage[i]);

C = (1.0/(double(size)))*SUMn;

beta = beta1;
f = 0;
do
{
    for(k=1; k<=3; k++)
    {
        A[k] = 0.0;
        for(i=1; i<=size; i++)
            A[k] = A[k] + ((pow(voltage[i], beta))*(pow(log(voltage[i]), k-1)));
    }

    f = (A[2]/A[1]) - (1.0/beta) - C;

    dif = (A[3]/A[1]) - ((A[2]/A[1])*(A[2]/A[1])) + (1.0/(beta*beta));

    beta = beta - (f/dif);
}
while(abs(f)>=0.0001);

//CALCULATE NEW A[1]. A[2] & A[3]
for(k=1; k<=3; k++)
{
    A[k] = 0.0;
    for(i=1; i<=size; i++)
        A[k] = A[k] + ((pow(voltage[i], beta))*(pow(log(voltage[i]), k-1)));
}

alpha = pow(((A[1]/double(size))), (1.0/beta));

cout<<"ALPHA = "<<alpha<<endl;
cout<<"NEW BETA = "<<beta<<endl;

//-----

WU = 1.63617 - (0.027229 * double(size)) + (5.7899e-4 * double(pow(size, 2)))

```

```

double(pow(size. 3)))
double(pow(size. 4)):
betaUP = WU * beta;
WL = 1.0/( 1.08509 + (6.89715/double(size))
+ (13.5325/double(pow(size, 2)))
+ (15.17619/double(pow(size, 3))) );
betaLOW = WL * beta;

Zurn = 0.11254 + (7.03279/double(size))
- (34.29964/double(pow(size, 2)))
+ (135.38431/double(pow(size, 3)))
- (90.73569/double(pow(size, 4)));

ZU = 0.17 + (Zurn - 0.17);

ZL = 0.10964 + (7.33402/double(size))
- (17.70106/double(pow(size, 2)))
+ (41.43168/double(pow(size, 3)));

alphaUP = alpha * exp(ZU/beta);
alphaLOW = alpha * exp((-1.0)*(ZL/beta));

cout<<endl;
cout<<"BETA RANGE : "<<betaLOW<<" < "<<"beta"<<" < "<<betaUP<<endl;
cout<<"ALPHA RANGE: "<<alphaLOW<<" < "<<"alpha"<<" < "<<alphaUP<<endl;

//-----
return;
} //END OF MAIN

//-----
//FUNCTION DEFINITAION FOR A FUNCTION THAT PUTS THE CONENTS OF
AN ARRAY IN
//ASCENDING ORDER
void selection_sort(double voltage[], int size)
{
int a, b, minidx;
double min, temp;

```

```
for(a=1; a<=(size-1); a++)
{
    min = voltage[a];
    minidx = a;
    for(b=a+1; b<=size; b++)
    {
        if(voltage[b]< min)
        {
            min = voltage[b];
            minidx = b;
        }
    }
    if (min < voltage[a])
    {
        temp = voltage[a];
        voltage[a] = min;
        voltage[minidx] = temp;
    }
}

return;
} //END OF selection_sort

//-----
```

## BIBLIOGRAPHY

- [1] Handbook of Electrical and Electronic Insulating Materials. Second Edition, W. Tillar Shugg, 1995.
- [2] Electricity and Magnetism, Prentice Hall, Ralph P. Winch, 1955.
- [3] Handbook of Statistical Methods for Engineers and Scientists, Second Edition, 1997.
- [4] Statistical Models and Methods for Lifetime Data, J. F. Lawless, 1982.
- [5] A graphical estimation of mixed Weibull parameters in life testing of electron tubes, Kao, J.H.K. Technometrics 1959. 389-407
- [6] Parameter estimation for the Weibull distribution, G.C.Stone and G.Van Heeswijk, IEEE Trans.Electr.Insul. vol E1-12 No.4, August 1977.
- [7] Estimating the Cumulative Probability of Failure Data Points to be Plotted on Weibull and other Probability Paper, J.C.Fothergill, IEEE Transaction of Electrical Insulation Vol 25, No.3. June 1990.
- [8] Introductory Engineering Statistics 3<sup>rd</sup> Edition, Irwin Guttman, S.S.Wilks, J.Stuart Hunter. pp.330 – 333, 1982.
- [9] “Maximum likelihood estimation in the Weibull distribution based on complete and on censored samples” .A.C.Cohen. Technometrics. vol.7, Nov 1965, pp579-588.
- [10] “Inferences on the Parameters of the Weibull Distribution”, D.R.Thoman, L.J.Bain and C.C.Antle, Technometrics, Vol. 2, No. 3, August 1969.
- [11] Electrical Degradation and Breakdown in Polymers, L.A.Dissado. J.C.Fothergill, pp443-444. 1992.

- [12] The Theory of Dielectric Breakdown of Solids, J.J.O'Dwyer 1964.
- [13] Dielectric breakdown and electrical conduction of poly(vinylidene-flouride) in high temperature region. M Hikita, M Nagao, G Sawa and M Ieda, J.Phys.D:Appl.Phys..13(1980) 661-6.
- [14] Conduction and Thermally Stimulated Discharge Currents in Aramid Paper, G R Raju, IEEE Transactions on Electrical Insulation, vol.27 No.1 pp162-172. Feb1992
- [15] Dielectric Breakdown of Polyimide Film in High Temperature Region, Masayuki Nagao, Goro Sawa, Masahiko Fukui and Masayuki Ieda, Japan. J.Appl.Phys.Vol.15 (1976). No.9 pp1813-1814.
- [16] Engineering Dielectrics, Volume IIA, Electrical Properties of Solid insulating Materials: Molecular Structure and Electrical Behavior, Bartnikas / Eichorn pp449, 1983.
- [17] Dielectric Breakdown of Solids, S Whitehead. 1951
- [18] Electrical Conduction in Kapton Polyimide Film at High Electric Fields, B.L.Sharma, Polymer 1982, Vol 23, January, pp17 –19
- [19] Electrical Conduction in Fluoropolymer Films, Z Leo and G. R. Govinda Raju, IEEE Transactions on Dielectrics and Electrical Insulation, Vol. 2 No. 3, June 1995.
- [20] Theory of Dielectrics, Second Edition, H. Frohlich, 1958
- [21] High Voltage Engineering E.Kuffel, W.S.Zaengl, 1984

## VITA AUCTORIS

NAME: Syed Zaki Jafri

DATE OF BIRTH: 18<sup>th</sup> March 1971

PLACE OF BIRTH: Karachi, Pakistan

EDUCATION: 1986 – 1988 Berkhamsted School, Hertfordshire, UK.

1989 – 1992 Imperial College of Science and Technology  
University of London, London, UK  
Bachelors of Electrical and Electronic Engineering

1997 – 2001 University of Windsor  
Windsor, Ontario, Canada.  
Master of Applied Science

WORK HISTORY: 1993 – 1996 Project Engineer  
AEG Daimler Benz Group  
Karachi, Pakistan

1999 – Date Project Manager  
KVT Technologies Inc.  
Oldcastle, Ontario, Canada